


Spin fluctuations and superconductivity in $Y_5Rh_6Sn_{18}$ doped with Pd and Co: Evidence of peak effect in the superconducting mixed state

A. Ślebarski ^{1,2,*}, M. Fijałkowski,^{3,2} and M. M. Mańska⁴

¹*Institute of Low Temperature and Structure Research, Polish Academy of Sciences, Okólna 2, 50-422 Wrocław, Poland*

²*Centre for Advanced Materials and Smart Structures, Polish Academy of Sciences, Okólna 2, 50-422 Wrocław, Poland*

³*Institute of Physics, University of Silesia in Katowice, 75 Pułku Piechoty 1, 41-500 Chorzów, Poland*

⁴*Department of Theoretical Physics, Wrocław University of Science and Technology, Wybrzeże Wyspiańskiego 27, 50-370 Wrocław, Poland*



(Received 13 May 2022; accepted 12 August 2022; published 26 August 2022)

We performed a systematic study of the nonmagnetic skutterudite-related $Y_5Rh_6Sn_{18}$ superconductor, where the lattice disorder on the coherence length scale ξ additionally generates a nonhomogeneous, *high-temperature* superconducting phase with disorder-enhanced critical temperature T_c^* . We have previously discussed various possibilities of local atomic disorder; one of the possibilities is doping. Our present studies focus on the series of $Y_{5-\delta}(Rh_{5.5}M_{0.5})Sn_{18}$ compounds ($\delta \ll 1$), where the dopants $M = Co, Ir, Ru$, and Pd, when they are smaller (Co) or larger (Pd) than Rh, generate the *peak effect* in fields smaller than the critical field H_{c2} . This phenomenon manifests itself as a weak peak in the real and imaginary parts of ac susceptibility and is more distinct in magnetoresistance. Using a simple theoretical model, we demonstrate that the effectiveness of this mechanism depends not only on the magnitude of the difference between the size of the dopant and the host atom, but also on whether the dopant is smaller or larger. The agreement between this prediction and our experimental data strongly supports the impurity-based scenario of the observed peak effect. Magnetoresistance isotherms of the remaining samples ($M = Ir$ and Ru) with the radius of M being very similar to that of Rh show, however, a weak peak-effect-like behavior, which is mainly due to vacancies δ at Y sites, while the corresponding ac susceptibility isotherms exhibit a distinct peak at $H \sim H_{c2}$. This field-dependent χ_{ac} anomaly appears to be similar in nature to the peak effect; however, it cannot be attributed to pinning and appears to be an equilibrium property of the system. We also report the coexistence of spin fluctuations and superconductivity for $Y_5Rh_6Sn_{18}$ doped with Pd and Co.

DOI: [10.1103/PhysRevB.106.075145](https://doi.org/10.1103/PhysRevB.106.075145)

I. INTRODUCTION

Systematic studies of atomic-scale disorder in skutterudite-related superconducting compounds such as $R_3M_4Sn_{13}$ and $R_5M_6Sn_{18}$ ($R = Y, La, Lu$; $M = Co, Rh, Ru$) in the form of local defects, vacancies, and doping have received our attention, particularly due to observations of new superconducting phenomena in these materials [1]. Namely, our previous comprehensive investigations have shown that atomic disorder has a significant impact on the increase in the critical transition temperature T_c . We have documented that disorder on the coherence length scale ξ in these nonmagnetic quasiskutterudite superconductors additionally generates a nonhomogeneous, *high-temperature* superconducting phase T_c^* with $T_c^* > T_c$ [2] (dilute disorder scenario), while strong fluctuations of stoichiometry due to increasing doping can rapidly increase the superconducting transition temperature of the sample even to the value of $T_c^* \sim 2 \times T_c$ [3] (dense disorder scenario). This phenomenon seems to be characteristic of high-temperature superconductors [4,5], strongly correlated superconducting electron systems (SCESs) [6–12], and SnSb

topological superconductors [13] and recently has received renewed attention. This behavior clearly diverges from the theoretical predictions, where the doping of a superconductor most often leads to the reduction or complete extinction of superconductivity [14,15], depending on the nonmagnetic or magnetic nature of the dopant.

This novel phenomenon is qualitatively well modeled theoretically by Gastiasoro and Andersen [16] in both the dilute and dense disorder scenarios. The first, diluted disorder, regime was studied in the case of multiband superconductors, where impurity resonant states generate local density of states (LDOS) enhancements at the Fermi level, while the second scenario for dense disordered materials concerns dense disorder in conventional one-band superconductors.

We experimentally documented the stronger lattice stiffening of the inhomogeneous superconducting phase T_c^* with respect to the bulk phase T_c and proposed a phenomenological model that explains the relation $T_c^* > T_c$ [3]. This observation was also justified by measurements of the Grüneisen parameter Γ^* which for the locally inhomogeneous T_c^* phase obtained values greater than those of the respective Γ of the bulk T_c phase, as was reported in Ref. [3].

The effective increase in disorder by doping of $Y_{5-\delta}Rh_6Sn_{18}$ with metal M or by vacancies δ at Y sites could be a reason for the appearance of the peak effect

*Author to whom correspondence should be addressed: andrzej.slebarski@us.edu.pl

(PE) in the system of $(Y_{4.5}M_{0.5})Rh_6Sn_{18}$ superconductors. Very recently, we reported that the PE can be observed when the radius of dopant M is smaller than that of Y. Alternatively, PE results from the presence of a vacancy at the Y sites. The aim of the current study is to show to what extent impurities in the crystallographic sites of Rh could change the superconductivity of $Y_5(Rh_{5.5}M_{0.5})Sn_{18}$ [17] and thus whether they generate similar magnetic-field-induced reentrance of superconductivity. In this paper, we have confirmed that the main cause of the PE phenomenon is the impurity M size with respect to Y or Rh, and the effect is independent of whether M is at the Y or Rh sites; therefore the current investigations are a significant supplement to the results published earlier in Ref. [18]. The magnetic-field-induced reentrance of superconductivity observed in the quasiskutterudites doped with M (or with vacancies δ) seems to be universal, dependent only on local defects (stresses).

Moreover, for the $M = Pd$ and Co dopants, the coexistence of superconductivity and spin fluctuations (SFs) has been observed; complex behavior such as this has rarely been reported for superconducting materials and suggests that the doped system is near the quantum critical point. Magnetic spin fluctuations are usually observed in materials close to the phase boundary of magnetic order and have a negative impact on superconductivity of the BCS type. The coexistence of superconductivity and spin fluctuations was first discovered in UPt_3 [19]. There are an increasing number of novel heavy-fermion superconductors for which superconductivity appears near the quantum critical point (QCP), $CePd_2Si_2$ and $CeIn_3$ [20], or UGe_2 [21], are good examples; the latter exhibits superconductivity in the limited pressure range. However, it is rare that the material exhibits both spin fluctuations and superconductivity without the Ce or U element. An example of such unique material with competition between superconductivity and spin fluctuations can be a skutterudite-related single crystal of $Ca_3Ir_4Sn_{13}$ [22] with non-Fermi-liquid behavior, which crystallizes in the $Pm\bar{3}n$ space group. For intermediate compositions $(Ca_xSr_{1-x})_3Ir_4Sn_{13}$ of this intriguing (3 : 4 : 13)-type superconductor, a novel structural quantum phase transition has even been reported as a result of negative chemical pressure from partial substitution of Ca by Sr, together with positive applied external pressure [23]. Here, we document that the anomalies in susceptibility, electrical resistivity, and specific heat of $Y_5Rh_6Sn_{18}$, when it is doped with Pd or Co, can also be understood within the framework of spin fluctuations.

II. EXPERIMENTAL DETAILS

The $Y_5(Rh_{5.5}M_{0.5})Sn_{18}$ polycrystalline samples were prepared using the arc-melting technique and then annealed at $870^\circ C$ for 2 weeks. The samples were examined by x-ray diffraction (XRD) analysis (PANalytical Empyrean diffractometer equipped with a $Cu K\alpha_{1,2}$ source) and found to have a tetragonal structure (space group $I4_1/acd$) [24,25]. The XRD patterns were analyzed with the Rietveld refinement method using the FULLPROF SUITE set of programs [26]. Stoichiometry and homogeneity were checked using an electron microprobe technique (scanning microscope JSM-5410).

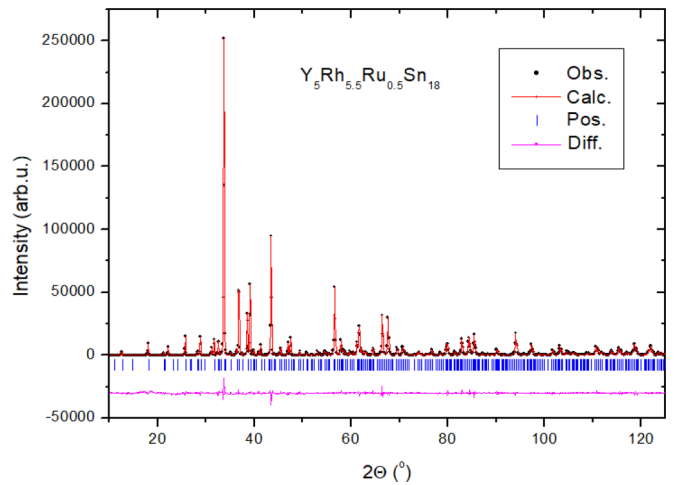


FIG. 1. Plot of Rietveld refinement for $Y_5Rh_{5.5}Ru_{0.5}Sn_{18}$. Black dots, observed pattern; red line, calculated pattern; blue ticks, Bragg peaks positions (Pos.); magenta line, the difference (Diff.) between observed and calculated patterns.

The x-ray photoelectron spectroscopy (XPS) spectra were obtained at room temperature with monochromatized Al $K\alpha$ radiation using a PHI 5700/600 ESCA spectrometer. To obtain good-quality XPS spectra, the samples were cleaved and measured in a vacuum of 6×10^{-10} Torr. The spectra were calibrated according to Ref. [27], and binding energies were referenced to the Fermi level ($\epsilon_F = 0$).

Electrical resistivity ρ was investigated using a conventional four-point ac technique using a Quantum Design Physical Properties Measurement System (PPMS). Thermodynamic investigations were performed using a PPMS platform. Specific heat C was measured in the temperature range 1.8–300 K and in external magnetic fields up to 5 T. The ac susceptibility measurements in superposed dc magnetic fields have been performed up to 5 T. The ac magnetic susceptibility was also measured at different frequencies and with an ac amplitude of 2 Oe versus temperature. Magnetization σ was measured in magnetic fields up to 5 T using a vibrating sample magnetometer (VSM) option.

III. $Y_5Rh_{5.5}M_{0.5}Sn_{18}$, WHERE $M = Co, Ir, Ru$, AND Pd : MAGNETIC-FIELD-INDUCED REENTRANCE OF SUPERCONDUCTIVITY IN $Y_5Rh_6Sn_{18}$ DOPED WITH METAL M

A. Structural properties

The XRD data analysis was performed with the Rietveld technique [26]. The results from refining the XRD data, presented in Table I, were obtained with the weighted-profile R factors [28] $R_{wp} < 3\%$ and $R_{Bragg} < 2\%$.

Figure 1 shows a representative XRD pattern for $Y_5Rh_{5.5}Ru_{0.5}Sn_{18}$ with Rietveld refinements. The unit cell volume of $Y_5Rh_{5.5}M_{0.5}Sn_{18}$ has a linear scaling with the atomic radius of metal $M = Co, Ir, Ru$, and Rh (as shown in Fig. 2), suggesting that the content of M is similar (of about 0.5 atoms/f.u.) in each component of the series, as was assumed. The atomic radii values were obtained from Ref. [29]. The energy-dispersive x-ray spectroscopy (EDXS)

TABLE I. Parameters obtained from the structural characterization of $Y_5(Rh_{5.5}M_{0.5})Sn_{18}$ superconductors.

$Y_5(Rh_{5.5}M_{0.5})Sn_{18}$ M	Lattice parameters (Å)	V (Å ³)	R_{wp} (%)
Co	$a = 13.7748(9), c = 27.4135(6)$	5201.66(1)	2.74
Ir	$a = 13.7697(7), c = 27.5280(5)$	5219.49(8)	2.67
Ru	$a = 13.7610(9), c = 27.5247(5)$	5212.29(9)	1.94
Rh	$a = 13.7601(2), c = 27.5412(3)$	5214.68(2)	2.7
Pd	$a = 13.8014(5), c = 27.5136(3)$	5240.79(8)	2.81

measurements indicate for the components M of the series a deficiency of Y and a similar excess of Sn with a composition of the samples close to $Y_{4.6}Rh_{5.5}M_{0.5}Sn_{18.5}$, when the content of Rh is normalized to 5.5 atoms/f.u. As an example, we present the EDXS composition $Y_{4.60}Rh_{5.5}M_{0.52}Sn_{18.80}$ for a Pd-doped sample. Similar off-stoichiometry had also been documented for various $(Y_{4.5}M'_{0.5})Rh_6Sn_{18}$ samples [18], which seems to be characteristic of a number of similar isostructural quasiskutterudites, obtained as polycrystals [30,31] as well as single crystals [32]. Previously, we documented both in the *ab initio* calculations and experimentally that the presence of vacancies in the 32(g) sites significantly modifies the band structure of the 5 : 6 : 18 system near the Fermi level [31]. As a result, different behaviors are observed for the compound under consideration, especially in the electron transport properties, which resulted only from a subtle change in the stoichiometry of the (5 : 6 : 18)-type system (cf. Ref. [33]). For example, our band structure calculation carried out for isostructural off-stoichiometry $Lu_{4.6}Rh_6Sn_{18}$ documented its semimetallic nature in the normal state, explicitly visible in the temperature variation of the resistivity $\rho(T)$ for $T > T_c$, while its stoichiometric equivalent $Lu_5Rh_6Sn_{18}$ is metallic. Continuing, EDXS research suggests a semimetallic character of the $Y_{5-\delta}Rh_6Sn_{18}$ samples doped with metal M either in the Y or Rh sites. The EDXS also indicates the nanoscale inhomogeneity on the length scale compared with

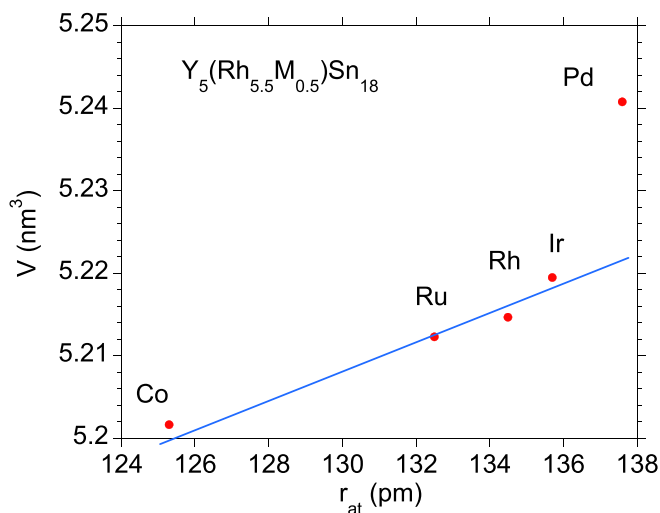


FIG. 2. Cell volumes for the series of the $Y_5(Rh_{5.5}M_{0.5})Sn_{18}$ compounds vs atomic radius of metal M taken from Ref. [29].

the coherence length ξ as a bulk property of these superconducting materials. This local inhomogeneity in $Y_5Rh_6Sn_{18}$ due to the local atomic disorder as well as an inhomogeneous doping effect is a reason for the appearance of the *high-temperature inhomogeneous superconducting phase* with critical temperature $T_c^* > T_c$, and was discussed in Refs. [1,2] and modeled by Gastiasoro and Andersen [16].

Figure 2 shows the unit cell volume for the series of $Y_5(Rh_{5.5}M_{0.5})Sn_{18}$ compounds as a function of the atomic radius of the dopants M . As shown in the figure, the unit cell volume of $Y_5Rh_{5.5}Pd_{0.5}Sn_{18}$ is $\sim 0.38\%$ higher than that expected by Vegard's law, although the stoichiometry obtained is very similar for all M components of the series. Therefore an anomalous increase in the volume of the Pd sample is not entirely understandable (one can also note a slightly larger volume of the Co sample than is expected). One can only suggest that the enhancement of the unit cell volume could be due to stronger spin fluctuations (SFs) generated by the Pd impurities (this will be discussed later).

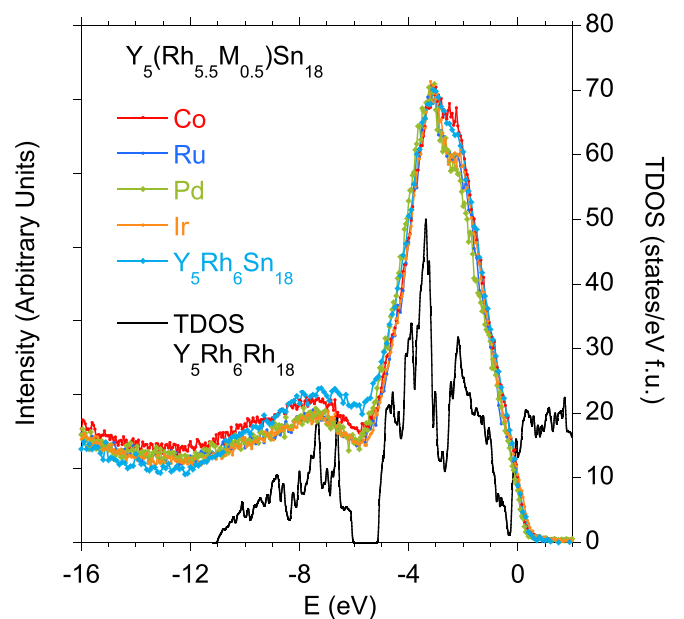


FIG. 3. Valence band XPS spectra for $Y_5(Rh_{5.5}M_{0.5})Sn_{18}$ are compared with the calculated total DOS for pristine $Y_5Rh_6Sn_{18}$ (TDOS values for $Y_5Rh_6Sn_{18}$ are taken from Ref. [34]). The intensities of all measured XPS bands are normalized to the background for $Y_5Rh_6Sn_{18}$ at $E > \epsilon_F$.

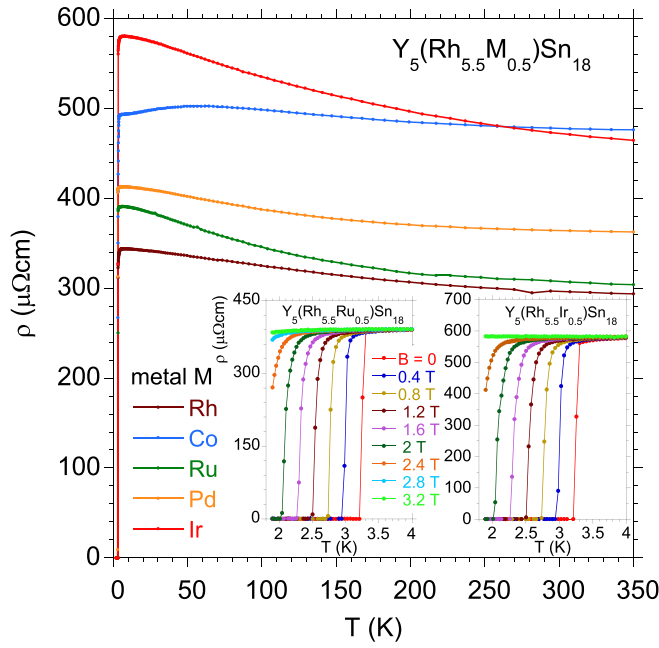


FIG. 4. Electrical resistivity ρ as a function of temperature ($B = 0$) for the series of $Y_5(\text{Rh}_{5.5}M_{0.5})\text{Sn}_{18}$, where $M = \text{Co}, \text{Ir}, \text{Ru}, \text{Rh}$ and Pd , with $\rho \sim T^{-1/4}$ behavior in the temperature range between ~ 80 and $\sim 300\text{--}350$ K, depending on the sample. The insets show details of $\rho_B(T)$ in the superconducting state for $Y_5\text{Rh}_{5.5}\text{Ru}_{0.5}\text{Sn}_{18}$ (left) and $Y_5\text{Rh}_{5.5}\text{Ir}_{0.5}\text{Sn}_{18}$ (right).

B. Valence band XPS spectra

Figure 3 compares the valence band (VB) XPS spectra of $Y_5(\text{Rh}_{5.5}M_{0.5})\text{Sn}_{18}$ with respect to the total density of states (TDOS) calculated for $Y_5\text{Rh}_6\text{Sn}_{18}$ ($M = \text{Rh}$). For details of *ab initio* calculations, we refer the reader to Ref. [34]. The most important conclusions from the comparison of the calculated and experimentally obtained bands are as follows. (i) The Rh 4d electron states dominate the VB XPS bands between the Fermi level ϵ_F and the binding energy -5 eV, while the Sn 5s states make a significant contribution to the VB XPS spectra between -6 and -11 eV. (ii) Dopants M do not significantly change the XPS valence bands, giving only a small contribution to the TDOS at about 2 eV [35] which, however, is not decisive for electric transport properties, while a deep hybridization pseudogap at approximately -0.3 eV has a significant impact on the conductivity in the normal state of each sample. (iii) We also documented that this hybridization pseudogap does not depend on the dopant M [18], while it is shifted toward ϵ_F by vacancies at the Y sites. Therefore the $Y_{5-\delta}\text{Rh}_6\text{Sn}_{18}$ and similar off-stoichiometry isostructural systems exhibit either semimetallic or metallic behavior at $T > T_c$, depending on the number of vacancies (cf. Refs. [18,31]).

C. Resistance variation as a function of applied field and measuring current

Figure 4 shows the resistivity of the $Y_5(\text{Rh}_{5.5}M_{0.5})\text{Sn}_{18}$ superconductors with a characteristic resistivity drop at T_c^* to the superconducting state ($T_c^* \gtrsim T_c$; cf. Table II). The characteristics $\rho(T)$ indicate several interesting effects in both the

TABLE II. Superconducting-state and normal-state (n) quantities for $Y_5(\text{Rh}_{5.5}M_{0.5})\text{Sn}_{18}$: electronic specific heat coefficient $\gamma_0^{(n)}$ obtained from the best fit of the expression $C(T)/T = \gamma_0^{(n)} + \beta T^2 + \eta T^2 \ln(T/I_{SF})$ to the experimental data for $B = 0$ [where $\beta = N(12/5)\pi^4 R \theta_D^{-3}$, N being the number of atoms per formula unit, and η determines the contribution of spin fluctuations in C if T_{SF} is assumed 1 K] (values in $\text{erg}/\text{cm}^3 \text{K}^2$ are given in parentheses), parameter η , Debye temperature θ_D , normal-state residual resistivity $\rho_n(0)$ approximated to $T = 0$, $n^{2/3} \frac{S}{S_F}$ calculated from Eq. (1), mean free path $l(0) = 1.27 \times 10^4 [\rho_n(n^{2/3} S/S_F)]^{-1}$, GLAG coherence length ξ_{GL}^{fv} (where fv refers to full value [50]), BCS coherence length $\xi^{BCS}(0) = 7.95 \times 10^{-17} (n^{2/3} \frac{S}{S_F})^{-1} (\gamma_0 T_c)^{-1}$, GLAG penetration lengths $\lambda_{GL}^{fv}(0)$ [50], Ginzburg-Landau parameter $\kappa_{GL}^{fv}(0)$, critical temperatures T_c and T_c^* (the initial temperatures of the formation of the percolation path are in parentheses), $\frac{dH_{c2}}{dT}$ in T_c and $\frac{dH_{c2}}{dT}$ at T_c^* , and the electron-phonon coupling parameters λ and λ^* for the T_c and T_c^* phases, respectively.

$Y_5(\text{Rh}_{5.5}M_{0.5})\text{Sn}_{18}$	$\gamma_0^{(n)}(B=0)$ (mJ/mol K ²)	η (J/mol K ⁴)	θ_D (K)	$\rho_n(0)$ (10 ⁻⁶ Ωcm)	$n^{2/3} \frac{S}{S_F}$ (10 ¹³ cm ⁻²)	$l(0)$ (nm)	$\xi_{GL}^{fv}(0)$ (nm)	$\xi^{BCS}(0)$ (nm)	$\lambda_{GL}^{fv}(0)$ (nm)	$\kappa_{GL}^{fv}(0)$	T_c (K)	T_c^* (K)	$\frac{dH_{c2}}{dT}$ (10 ⁴ G/K)	$\frac{dH_{c2}^*}{dT}$ (10 ⁴ G/K)	λ	λ^*
Co	20.0 (536)	0.0015	173	493	4.6 (6.1 ^a)	6 (4 ^a)	8 (8 ^a)	22 (29 ^a)	998	103	3.08	3.15 ^a (3.83)	-1.785	-1.626 ^a	0.48	0.48 ^a
Ir	9.4 (239)	0	156	581	1.2 (1.3 ^a)	18 (17 ^a)	7 (8 ^a)	13 (13 ^a)	1520	208	3.18	3.25 ^a (3.85)	-1.888	-1.726 ^a	0.49	0.50 ^a
Ru	9.9 (252)	0	154	392	1.1 (1.3 ^a)	29 (25 ^a)	8 (8 ^a)	11 (13 ^a)	1562	217	3.08	3.24 ^a (4.04)	-2.100	-1.759 ^a	0.49	0.50 ^a
Rh	13.0 (331)	0	164	343	1.6 (1.7 ^a)	23 (22 ^a)	8 (8 ^a)	12 (13 ^a)	1293	170	3.08	3.19 ^a (3.82)	-1.895	-1.713 ^a	0.48	0.49 ^a
Pd	28.0 (710)	0.001	176	413	5.8 (11.2 ^a)	5 (3 ^a)	8 (8 ^a)	24 (43 ^a)	965	121	2.67	2.92 ^a (3.45)	-1.921	-1.655 ^a	0.46	0.47 ^a

^a Assigned to the inhomogeneous high-temperature T_c^* phase.

superconducting and the *normal metallic* (n) state. (i) The $\rho(T)$ behavior in the n state is semimetallic and exhibits a negative temperature coefficient (TCR) $d\rho/dT < 0$ in a wide temperature range of $100 \text{ K} \lesssim T \lesssim 350 \text{ K}$ with $\ln \rho \sim T^{-1/4}$ dependence (not shown here). In this T range we observed an agreement of $\rho(T)$ with the Mott variable-range hopping effect; $\rho \propto \exp[(\frac{\Delta_M}{k_B T})^{1/4}]$ [36,37], where Δ_M is a pseudogap in the band structure near the Fermi level. Indeed, *ab initio* calculations documented the presence of the deep pseudogap for $\text{Y}_5\text{Rh}_6\text{Sn}_{18}$ [3,34], isostructural $\text{Lu}_5\text{Rh}_6\text{Sn}_{18}$ [18], and other similar isoelectronic quasiskutterudites with stoichiometry $3 : 4 : 13$ [30,38], at a binding energy of approximately -0.3 eV . The shape of this pseudogap is not changed by doping [18], while even a small number of vacancies shifts the pseudogap towards the Fermi level; simultaneously, the presence of defects may reduce the pseudogap after its shift to ϵ_F (this is a characteristic behavior of Kondo insulators; see, e.g., Ref. [39]). Semimetallic $\rho(T)$ behavior (shown in Fig. 4) with accompanying Mott variable-range hopping effects in the metallic state of $\text{Y}_5(\text{Rh}_{5.5}M_{0.5})\text{Sn}_{18}$ is interpreted here as being a consequence of vacancies at Y sites.

The normal-metallic-state properties of Co- and Pd-doped samples are indicative of spin-fluctuation phenomena. A T^2 term in resistivity, a broad maximum in the real component of ac magnetic susceptibility χ_{ac} , and a $T^3 \ln T$ contribution to the specific heat give strong evidence for the coexistence of spin fluctuations and bulk superconductivity near the critical temperature, which makes these compounds unique materials. To start with the first piece of evidence, Fig. 5 displays the ρ vs T^2 dependence above T_c^* for $\text{Y}_5\text{Rh}_{5.5}\text{Co}_{0.5}\text{Sn}_{18}$ (upper panel) and $\text{Y}_5\text{Rh}_{5.5}\text{Pd}_{0.5}\text{Sn}_{18}$ (lower panel) in a limited temperature range, in order to compare the ρ data with predictions of the theory of Ueda and Moriya [40,41]. The data in the temperature range ΔT —from T_c^* to 30 K for $M = \text{Co}$ and from T_c^* to 8 K for the Pd dopant—fit very well the T^2 law regarding the scattering of carriers on spin fluctuations. The resistivity in the superconducting state is shown in detail in Figs. 4 and 6-8. For dopants $M = \text{Ir}, \text{Ru},$ and Rh , with an atomic radius similar to that of Rh , $\rho_B(T)$ exhibits a sharp drop below T_c^* with the transition width being less than 0.1 K, which attests to the good quality of the polycrystals (as shown in the insets of Fig. 4 and also in Fig. 10(a) of Ref. [18]). A broadening of the transition with increasing magnetic fields is observed until the superconducting state completely disappears at fields larger than the critical field H_{c2} . Similarly, magnetoresistance isotherms $\rho_T(B)$ for $\text{Y}_5(\text{Rh}_{5.5}M_{0.5})\text{Sn}_{18}$ ($M = \text{Ir}, \text{Ru}, \text{Rh}$) are typical of BCS superconductors, as shown in Fig. 7, and do not present any feature with nonzero resistivity at lower fields; this is also the case for the Pd-doped sample. The maxima in derivatives $d\rho_T/dB$ mark only a slight change in the slope of isotherms $\rho_T(B)$ at $T_c^*(B)$, which signals anomalies in the field-dependent ac magnetic susceptibility (which will be discussed). Here, one can observe that the atomic radius of metal M is comparable to that of the rhodium one. In contrast, the characteristics $\rho_B(T)$ for the Co and Pd samples are broad at the superconducting transition at T_c^* [as shown in Figs. 6(a) and 7(d)], especially under the zero magnetic field, which we associate with the coexistence of superconductivity and spin fluctuations. Moreover, peak effect anomalies in the resistivity of $\text{Y}_5\text{Rh}_{5.5}\text{Co}_{0.5}\text{Sn}_{18}$ are clearly seen in the variation of ρ

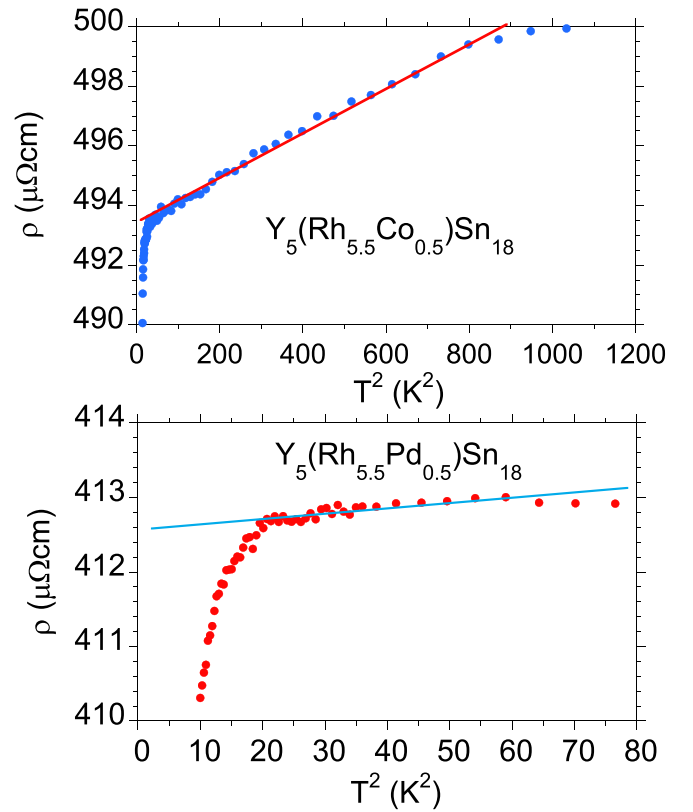


FIG. 5. A T^2 dependence of $\rho(T)$ in the normal metallic state for $\text{Y}_5\text{Rh}_{5.5}\text{Co}_{0.5}\text{Sn}_{18}$ ($T_c < T < 30 \text{ K}$) and for $\text{Y}_5\text{Rh}_{5.5}\text{Pd}_{0.5}\text{Sn}_{18}$ ($T_c < T < 8 \text{ K}$). The straight lines show a T^2 dependency.

vs magnetic field under various measuring current. Here, one notes that the difference between the Co and Rh atomic radii is the largest within the series of $\text{Y}_5(\text{Rh}_{5.5}M_{0.5})\text{Sn}_{18}$ superconductors (see Fig. 2); as a result of doping with the largest Co atom, a stronger local lattice stress appears. However, this field-dependent behavior is no longer so clearly visible for the remaining $\text{Y}_5(\text{Rh}_{5.5}M_{0.5})\text{Sn}_{18}$ samples (cf. Fig. 8), where the size of atom M is comparable to that of Rh . A detailed analysis of the characteristics of $\rho_T(B)$ for $\text{Y}_{5-\delta}(\text{Rh}_{5.5}M_{0.5})\text{Sn}_{18}$ shows only a weak nonzero resistivity tail for larger currents in lower fields. This peak-effect-like behavior is due to the presence of a small number of vacancies in the Y sites. A very similar behavior is also observed for $\text{Y}_{5-\delta}(\text{Rh}_{5.5}M_{0.5})\text{Sn}_{18}$ with Ir, Ru, and Pd dopants. Therefore it can be assumed that the weak peak-effect-like behavior is only generated by the presence of vacancies in the Y sites, when Rh atoms are partially replaced by dopants M with almost identical atomic radii. This suggests that small but finite resistivity arises in the superconducting state because of the current inducing a sufficiently large Lorentz force to cause the movement of vortices; however, the reason for this observation is not doping, but the presence of Y vacancies documented by EDXS. On the other hand, the unit cell volume of $\text{Y}_{5-\delta}\text{Rh}_{5.5}\text{Pd}_{0.5}\text{Sn}_{18}$ is significantly larger than the volume of $\text{Y}_{5-\delta}\text{Rh}_6\text{Sn}_{18}$ (cf. Fig. 2), which additionally causes the presence of weak PE at 1.9 K in a narrow range of fields and measuring current, as shown in Fig. 8 [the effect is not observed in $\rho_T(B)$ data at $T = 2.2$ and 2.5 K].

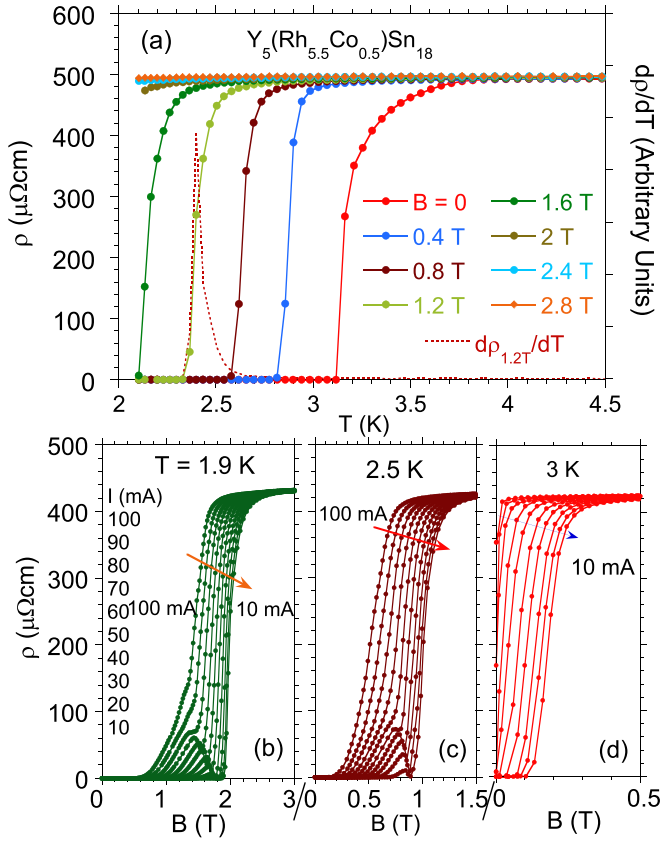


FIG. 6. (a) Electrical resistivity $\rho(T)$ for $Y_5Rh_{5.5}Co_{0.5}Sn_{18}$ below T_c at various magnetic fields, for a measuring current of 10.2 mA. (b)–(d) Isotherms of ρ for different measuring currents as a function of the magnetic field.

D. Thermodynamic characterization

Shown in Fig. 9 is the specific heat C of $Y_5Rh_{5.5}Pd_{0.5}Sn_{18}$ plotted as C/T in various magnetic fields. Analogous characteristics of $C(T)/T$ were determined for the remaining compounds; therefore these data are shown as an example. In the normal state, the low-temperature specific heat data, C/T , are well approximated by the expression $C(T)/T = \gamma_0^{(n)} + \beta T^2 + \eta T^2 \ln(T/T_{SF})$ [as shown in the inset of Fig. 9(a)], where $\gamma_0^{(n)}$ is a normal-state electronic specific heat coefficient, $\beta = N(12/5)\pi^4 R \theta_D^{-3}$ is the phonon coefficient (N is the number of atoms per formula unit), and the last term expresses the contribution from spin fluctuations (if parameter $\eta \neq 0$). For Pd- and Co-doped samples the SF contribution is weak but detectable [$\eta \sim 0.001 \pm (1.3 \times 10^{-5})$ J/mol K⁴], while for Ir-, Ru-, and Rh-doped samples $\eta = 0$ [42]. Figure 9(b) shows the specific heat isotherms $C_T(B)$ divided by T as a function of the magnetic field with linear behavior in fields lower than the critical field H_{c2} . Similar $C_T(B)$ characteristics were observed for the remaining $Y_5(Rh_{5.5}M_{0.5})Sn_{18}$ compounds, which suggests for all samples the presence of s -wave one-band superconductivity.

Figure 9(c) shows the temperature dependence of the upper critical field H_{c2} plotted on the $H - T$ diagram for both the T_c and T_c^* phases of $Y_5Rh_{5.5}Ru_{0.5}Sn_{18}$. The $H - T$ data are well approximated by the Ginzburg-Landau equation $H_{c2}(T) =$

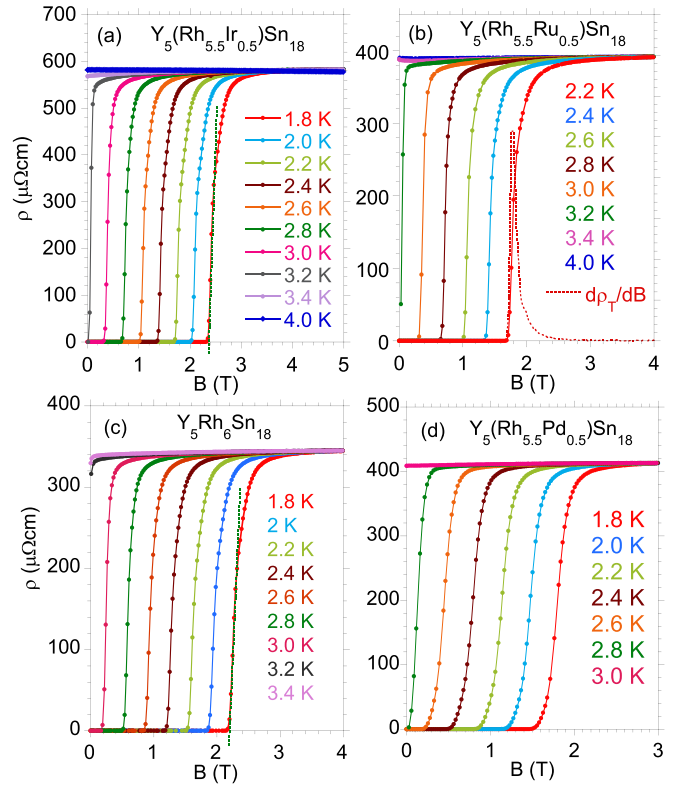


FIG. 7. Magnetoresistance isotherms for a measuring current of 10.2 mA as a function of applied magnetic field for $Y_5Rh_{5.5}Ir_{0.5}Sn_{18}$ (a), $Y_5Rh_{5.5}Ru_{0.5}Sn_{18}$ (b), $Y_5Rh_6Sn_{18}$ (c), and $Y_5Rh_{5.5}Pd_{0.5}Sn_{18}$ (d). In (a)–(c) a feature in the $\rho_T(B)$ curves (marked by a dotted line) at fields of about 2.2 T with accompanying maxima in $d\rho_T(B)/dB$ indicates the PE behavior (cf. Fig. 6).

$H_{c2}(0) \frac{1-t^2}{1+t^2}$ with $H_{c2}^* < H_{c2}$ and different $\frac{dH_{c2}}{dT}$ near the critical temperature T_c or T_c^* , respectively. Very similar $H - T$ plots were obtained for all samples investigated here (cf. Table II). We have already shown [1] that $H - T$ behavior such as this can be well approximated by the percolation model, assuming that the inhomogeneous system, where the local critical temperature $T_c^{(i)}$ is continuously spread over some inhomogeneous range, can be analyzed as a random resistor network (RRN) [43,44] and the dependence between $H_{c2}^{(i)}$ and $T_c^{(i)}$ is linear. The RRN model is also adequate to describe the $H - T$ dependencies for the series of $Y_5(Rh_{5.5}M_{0.5})Sn_{18}$ compounds.

On this occasion, it should be noted that the presence of the T_c^* phase is the result of a local disorder and local inhomogeneities related to doping. Alternatively, the phenomenon $T_c^* > T_c$ could be assigned to surface superconductivity. This was theoretically predicted [45] and confirmed by experiment [46]: Namely, a surface superconducting layer with critical field H_{c3} can exist above the bulk critical field H_{c2} when the external field is parallel to a sample surface; then $H_{c3} = 1.69H_{c2}$. For several reasons, this is not the case; the samples are polycrystalline, and always $H_{c2} > H_{c2}^*$, as shown in Fig. 9(c).

Figure 10 shows the frequency dependence of ac mass susceptibility χ_{ac} for $Y_5Rh_6Sn_{18}$ doped with Co [Fig. 10(a)] and Pd [Fig. 10(b)], respectively. The transition to the bulk superconducting state is very narrow for $Y_5Rh_{5.5}Co_{0.5}Sn_{18}$, while

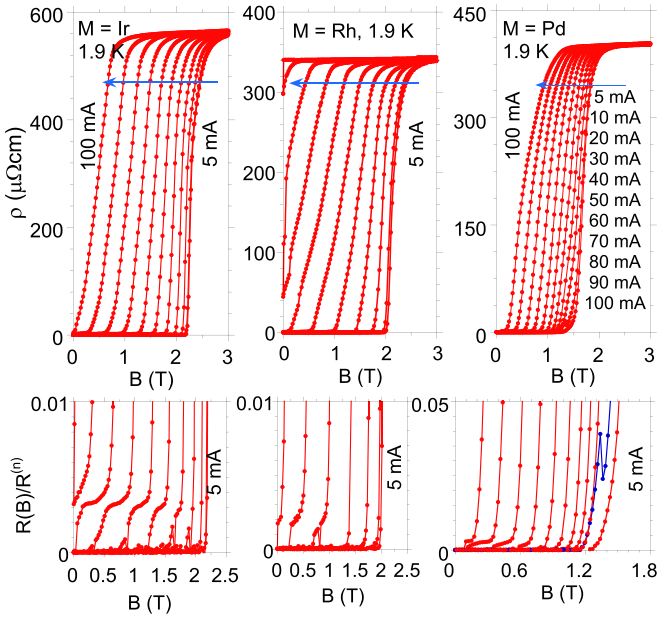


FIG. 8. Magnetoresistance isotherms at 1.9 K at various measuring currents as a function of applied magnetic field for $Y_5(\text{Rh}_{5.5}M_{0.5})\text{Sn}_{18}$, where $M = \text{Ir}$ (left upper panel), Rh (middle upper panel), and Pd (right upper panel). The lower panels show details of the change in resistance $R(B)/R^{(n)}$ at $T = 1.9$ K under applied magnetic field B for the samples doped with Ir , Rh , and Pd , respectively, where $R^{(n)}$ is the normal-state resistance at the field $B \gtrsim H_{c2}$ and measuring current 5 mA. Magnetoresistance of Pd -doped sample shows the PE at 1.9 K for a measuring current of 10 mA (blue points); the effect PE is not observed at $T = 2.2$ or 2.5 K.

between the critical temperature $T_c = 3.08$ K and ~ 3.8 K there is a second broad transition, which is related to the percolation nature of superconductivity. However, the derivative $d\chi'/dT$ allowed us to separate the bulk T_c and the inhomogeneous T_c^* superconducting phases (see Table II). Very similar $\chi_{ac}(T)$ characteristics are observed for dopants $M = \text{Ir}$, Ru , and Rh near T_c (not shown here), while χ_{ac} for $Y_5\text{Rh}_{5.5}\text{Pd}_{0.5}\text{Sn}_{18}$ exhibits a broad superconducting transition shown in Fig. 10(b) in the presence of SFs, clearly seen in the $\chi'(T)$ data at $T > T_c$. That is, χ' shows another broad maximum at ~ 12 K for the Pd -doped sample, as shown in the inset of Fig. 10(b). A similar feature in $\chi'(T)$ was also observed for the Co -doped sample at $T \sim 100$ K; these maxima, however, are not present in $\chi_{ac}(T)$ dependencies for the remaining $Y_5(\text{Rh}_{5.5}M_{0.5})\text{Sn}_{18}$ samples with the dopants $M = \text{Ir}$, Ru , and Rh . Figure 11 shows ac susceptibility as a function of temperature and applied dc magnetic field. The samples were initially cooled in a zero field to the required temperature, and then χ_{ac} was measured for an increasing or decreasing magnetic field B . The B variations of the real and imaginary parts of the ac magnetic susceptibility are shown for various $Y_5(\text{Rh}_{5.5}M_{0.5})\text{Sn}_{18}$ samples in Fig. 11. With increasing B , χ' continuously increases up to a field B^* (that is, $|\chi'|$ which decreases since $\chi' < 0$), while as the field increases further, it shows a peak. χ'' shows similar behavior, as shown in Fig. 11. The peak χ' is not frequency dependent, but shifts to lower fields with increasing T as well as with increasing radius of dopant M . We found that the atomic radius of M is

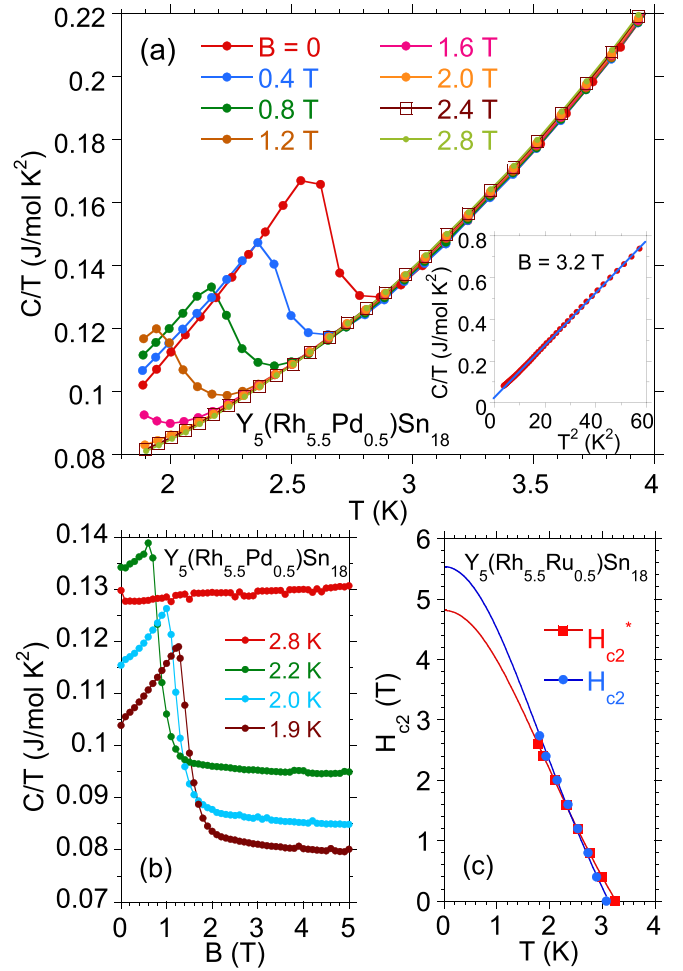


FIG. 9. Representative specific heat data for the series of $Y_5(\text{Rh}_{5.5}M_{0.5})\text{Sn}_{18}$. (a) Temperature dependence of specific heat, $C(T)/T$, for $Y_5\text{Rh}_{5.5}\text{Pd}_{0.5}\text{Sn}_{18}$ at various magnetic fields. The inset displays $C(T)/T$ data above T_c , well approximated by the expression $C(T)/T = \gamma_0^{(n)} + \beta T^2 + \eta T^2 \ln(T/T_{\text{SF}})$ with the following parameters ($B = 3.2$ T): $\gamma_0 = 0.038$ J/mol K^2 , $\beta = 0.010$ J/mol K^4 , and $\eta = 0.001$ J/mol K^4 (T_{SF} is assumed to be 1 K). (b) The C isotherms as a function of magnetic field B for $Y_5\text{Rh}_{5.5}\text{Pd}_{0.5}\text{Sn}_{18}$. (c) Temperature dependencies of the upper critical field for the bulk (T_c) and disorder (T_c^*) phases. The $H - T$ data are approximated by the Ginzburg-Landau (GL) model: $H_{c2}(T) = H_{c2}(0) \frac{1-t^2}{1+t^2}$ and $t = T/T_c$ (lines).

a reason of different efficiency of PE in both the resistance and susceptibility measurements. Namely, when the relative difference between the radii of M and Rh is small, the PE is very weak in the electrical resistance or even is not observed, while it becomes more pronounced in the susceptibility χ_{ac} measured in the external dc magnetic fields (compare Figs. 2, 4, 7, 8, and 11). Figure 11 shows a clear relationship between the maximum value of the real component χ' of the ac susceptibility and the value of the atomic radius of M . For $Y_5\text{Rh}_6\text{Sn}_{18}$ ($M = \text{Rh}$) the peak-effect-like behavior is found to be the largest, while for dopants with a smaller (Co , Ir , Ru) or larger (Pd) atomic radius in comparison to the Rh one, the amplitude of PE in the χ_{ac} data is systematically decreasing, reaching the smallest value for Co and Pd , respectively. This

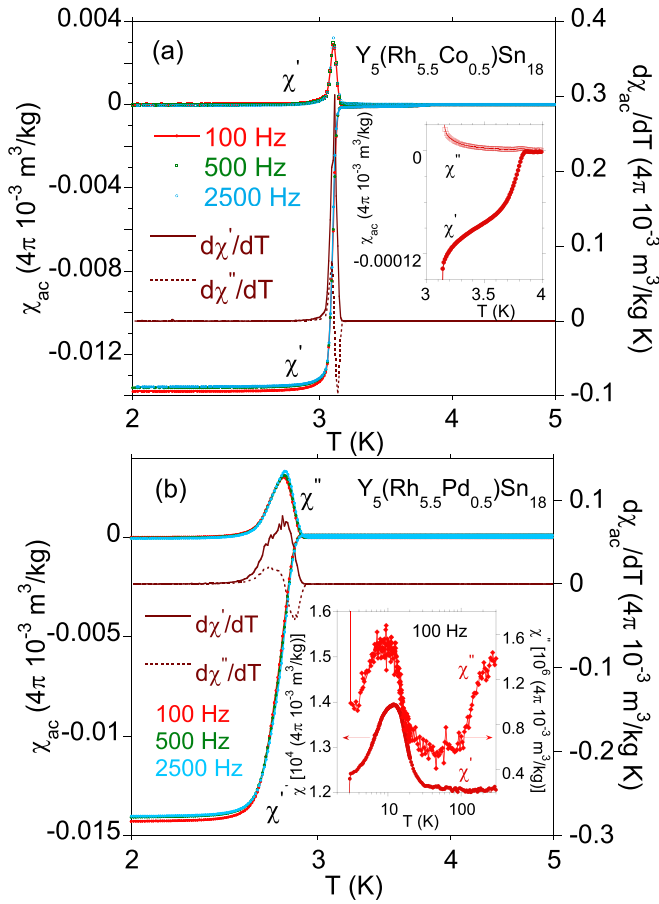


FIG. 10. Temperature dependencies (log scale) of the real χ' and imaginary χ'' components of the ac mass magnetic susceptibility χ_{ac} per 1 Oe for $Y_5Rh_6Sn_{18}$ doped with Co (a) and Pd (b), measured at different frequencies ν , and derivatives $d\chi'/dT$ and $d\chi''/dT$ (the unit used, $4\pi \times 10^{-3} \text{ m}^3/\text{kg}$ [Système International (SI)], is equivalent to 1 emu/g (cgs)). The inset in (a) shows a broad transition at 3.83 K to the state with separate superconducting regions, which, however, do not form a continuous path across the system. Similar $\chi_{ac}(T)$ behavior was observed for the remaining compounds (cf. Table II). The inset in (b) exhibits a maxima in χ_{ac} due to SFs.

anomaly in resistance measurements behaves in the opposite way; that is, for the Co dopants, the PE anomaly is observed to be the largest.

Figures 12 and 13 show the variation of the magnetization σ isotherms as a function of B . The σ vs B plots exhibit a peak in the magnetic field B^* before the upper critical field H_{c2} is reached. This behavior is characteristic of superconductors with PE due to the sudden increase in the current density below H_{c2} . The ac susceptibility and magnetization measurements indicate the presence of PE-like behavior, where in a certain field range near H_{c2} there is an increase in the critical current J_c with increasing field instead of a decrease, which also accounts for the observation of hysteresis between the up-sweeping and down-sweeping measurements (cf. the insets of Figs. 12 and 13). The hysteresis loops below T_c shown in Fig. 13 are characteristic of irreversible superconductivity.

Magnetization of the Pd-doped sample saturates in fields larger than 0.5 T giving at $T = 0$ the saturated magnetic

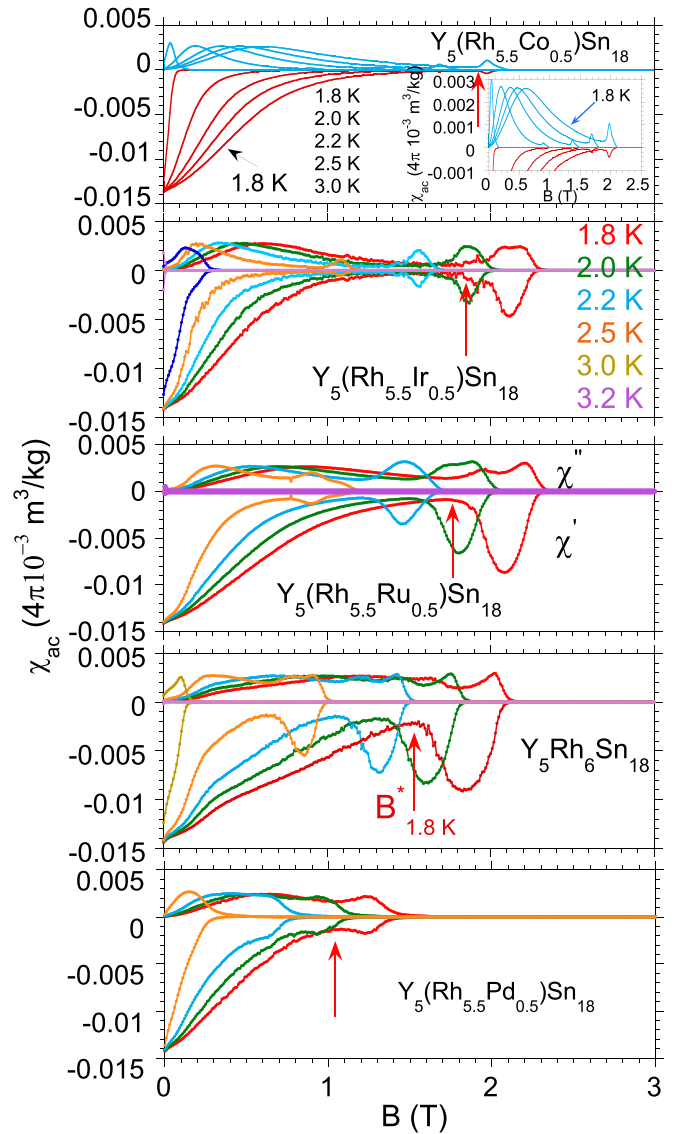


FIG. 11. Real (χ') and imaginary (χ'') parts of the ac susceptibility as a function of dc magnetic field at different temperatures [$4\pi \times 10^{-3} \text{ m}^3/\text{kg}$ (SI) is equivalent to 1 emu/g (cgs)]. The arrows indicate the field B_T^* at which the onset of the peak in the χ_{ac} isotherms occurs. The field B_T^* evidently depends on the atomic radius of dopant M (cf. Fig. 2).

moment per one Pd atom $\mu_s = 0.028 \mu_B/\text{Pd}$ atom, suggesting the presence of strong spin fluctuations. Similar values of μ_s per atom have been shown for other weak itinerant ferromagnets such as $ZrZn_2$ ($0.12 \mu_B/\text{Zr}$ atom [47]), $InSc_3$ ($0.045 \mu_B/\text{Sc}$ atom [48]), or superconducting Y_4Co_3/Y_9Co_7 ($0.012 \mu_B/\text{Co}$ atom [49]).

From these various experiments we obtained the parameters characteristic of the superconducting and normal states of $Y_5(Rh_{5.5}M_{0.5})Sn_{18}$ superconductors, based on theoretical predictions of the Ginzburg-Landau-Abrikosov-Gor'kov (GLAG) theory for type-II superconductivity; the most useful quantities are listed in Table II. According to Ref. [50], all parameters listed in Table II were calculated as a *full value*. The samples were found to be moderately dirty alloys with

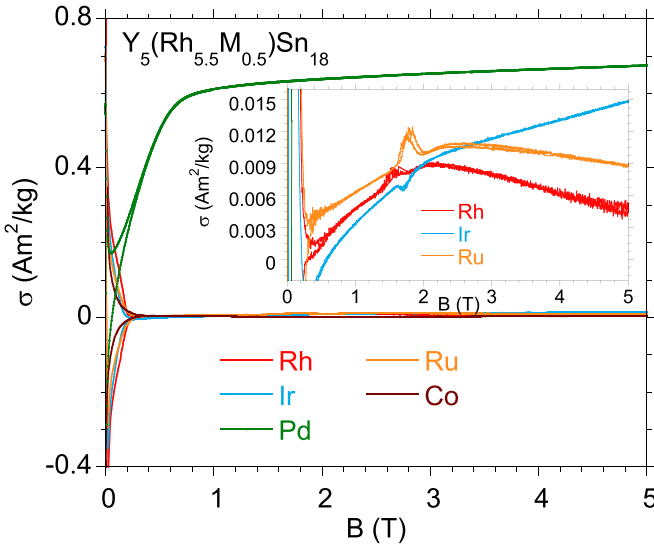


FIG. 12. Magnetization σ as a function of applied magnetic field at 2 K for a series of $Y_5(Rh_{5.5}M_{0.5})Sn_{18}$ compounds. The inset shows the details.

$\xi \approx l$. The slope of $\frac{dH_{c2}}{dT}$ obtained from the specific heat and resistivity data near the critical temperature T_c is a fundamental quantity for determining other parameters of the superconducting (SC) state. In the framework of the GLAG theory [51] the slope of $\frac{dH_{c2}}{dT}$ at T_c in units of gauss per kelvin is

$$-\left. \frac{dH_{c2}}{dT} \right|_{T=T_c} = \left[9.55 \times 10^{24} \gamma_0^2 T_c \left(n^{2/3} \frac{S}{S_F} \right)^{-2} + 5.26 \times 10^4 \gamma_0 \rho_n \right] [R(\lambda_{tr})]^{-1}, \quad (1)$$

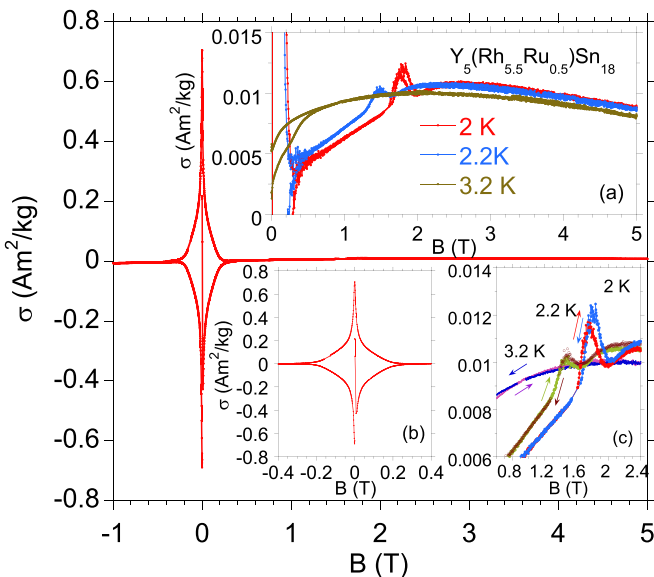


FIG. 13. Magnetization σ as a function of applied magnetic field at different temperatures for $Y_5Rh_{5.5}Ru_{0.5}Sn_{18}$. The insets show the details.

where n is the density of conduction electrons in cm^{-3} , S/S_F is the ratio of the real Fermi surface S to the surface $S_F = 4\pi(3\pi^2n)^{3/2}$ of the free electron gas, and the Gor'kov function $R(\lambda_{tr}) \approx 1$ for $\lambda_{tr} \rightarrow 0$ [$\lambda_{tr} \sim \xi(0)/l(0) \approx 0$ for all samples]. Then, the estimate of $n^{2/3}(S/S_F)$ allowed us to calculate the Ginzburg-Landau coherence length ξ_{GL}^{fv} , the GL penetration depth λ_{GL}^{fv} , and the GL parameter $\kappa_{GL}^{fv}(0)$. To calculate these parameters, we used the expressions in Ref. [50] (see also Ref. [18]).

The BCS theory gives

$$T_c = 1.14 \langle \omega \rangle \exp[-1/(N(\epsilon_F)U)], \quad (2)$$

where $N(\epsilon_F)$ is the density of states (DOS) at the Fermi energy in units of states/(eV spin), $\langle \omega \rangle \sim \theta_D/1.2$, and $N(\epsilon_F)U$ is approximately [52]

$$N(\epsilon_F)U \rightarrow \frac{\lambda - \mu^*}{1 + \lambda}. \quad (3)$$

Here, μ^* is the Coulomb pseudopotential given by Morel and Anderson [53]:

$$\mu^* = \frac{N(\epsilon_F)U}{1 + N(\epsilon_F)U \ln(E_B/\omega_0)}, \quad (4)$$

where E_B is the electronic bandwidth, ω_0 is the maximum phonon frequency, and λ is the electron-phonon coupling parameter [54,55]. By combining Eqs. (3) and (4), where $x = \ln(E_B/\omega_0)$ and $E_B \sim 4.5$ eV is the calculated conduction band width, we obtain the expression

$$N(\epsilon_F)U = \frac{-[2 + \lambda(1-x)] + [\lambda^2(1+x)^2 + 4\lambda + 4]^{1/2}}{2x(1+\lambda)}, \quad (5)$$

which was used to calculate λ 's and λ^* 's. Recently [31], we proposed a self-consistent procedure to calculate the λ 's from the best agreement between *experimental* values of $N(\epsilon_F)U$ and $[N(\epsilon_F)U]^*$ for the respective T_c and T_c^* phases given by expression (2) and λ -dependent variable $N(\epsilon_F)U$ from Eq. (5). In Table II the electron-phonon coupling parameters λ^* obtained for the inhomogeneous T_c^* superconducting phase by this self-consistent procedure are slightly larger than the λ 's of the respective bulk T_c superconducting state. This is a characteristic behavior of disordered quasiskutterudites (cf. Ref. [1]).

In summary, our extensive investigations of the class of $Y_5(Rh_{5.5}M_{0.5})Sn_{18}$ compounds have shown that atomic disorder, as well as an inhomogeneous doping effect, has a significant impact on both the increase in T_c and the nature of superconductivity. We experimentally documented that the effective increase in disorder caused by doping or vacancies is closer to a pressure effect and could be a reason for the appearance of a peak effect, which is first of all evident in resistivity data (also in susceptibility data) when the dopant M is smaller than Rh or is vacant. The most important results are summarized in Table II.

IV. SPIN FLUCTUATIONS AND SUPERCONDUCTIVITY IN $Y_5Rh_6Sn_{18}$ DOPED WITH Pd AND Co: COMMENTS

The low-temperature anomalies in specific heat (in Fig. 9), ac susceptibility (in Fig. 10), and resistivity (Fig. 5)

allowed a more likely interpretation of the experimental data for $Y_5Rh_{5.5}Pd_{0.5}Sn_{18}$ in terms of spin fluctuations. In the case of Co dopant, the effect is much weaker; however, it is clearly visible in the $\rho \sim T^2$ behavior as well as in the $\chi_{ac}(T)$ data. Therefore we will focus mainly on the results for the $Y_5Rh_6Sb_{18}$ sample doped with Pd. Theory [56–58] predicted the quenching of spin fluctuations in high magnetic fields. The quenching of spin fluctuations by magnetic fields has been observed, e.g., in the heat capacity C/T vs T measurements at low temperatures for several weak itinerant ferromagnets such as $LuCo_2$ [59], Sc_3In [60], and others, where the $T^3 \ln T$ term of the heat capacity disappears in fields larger than 2.5–5 T, depending on the system considered. The data shown in Fig. 14 support these predictions both for $Y_5Rh_{5.5}Pd_{0.5}Sn_{18}$ and $Y_5Rh_{5.5}Co_{0.5}Sn_{18}$ in fields higher than H_{c2} . Under applied fields $B < H_{c2}$ the Sommerfeld coefficient $\gamma(B)$ in the mixed state is found to follow a square-root field dependence. A similar $\gamma \sim B^{1/2}$ behavior is also observed for the remaining $Y_5(Rh_{5.5}M_{0.5})Sn_{18}$ samples in fields extended to 9 T, and without any deviation from the square-root field dependence, as shown in Fig. 14 [for the sample with Ir, $\gamma(B)$ deviates from the $B^{1/2}$ change in fields larger than 6 T, which could suggest a weak SF effect].

The field dependence of γ (in Fig. 14) is well approximated by $\gamma(B) = \gamma(0) + \gamma' B^{1/2}$, which is a sign of an anisotropic superconducting gap. Numerous previous measurements indicated that $Y_5Rh_6Sn_{18}$ has an anisotropic superconducting gap of point-node type [61–63]. In the case of nodes in the superconducting gap, Volovik predicted a nonlinear relation given by $\gamma(B) \propto B^{1/2}$ [64]. On the other hand, the γ of isostructural $Lu_5Rh_6Sn_{18}$ [61] and $Sc_5Rh_6Sn_{18}$ [65] superconductors shows a linear field dependence, which points to an isotropic superconducting gap. For fields $B > H_{c2}$, γ of samples doped with Pd and Co clearly decreases with increasing B , suggesting that the quenching of SFs by high magnetic fields dominates the $\gamma \propto B^{1/2}$ effect. In nearly magnetic materials, not only γ , but also β can be affected by spin fluctuations, where $\beta = \beta_L + \beta_\sigma(H)$ is a normal lattice β_L contribution and magnetic $\beta_\sigma(H)$ component. The C/T data for the Pd- and Co-doped samples did not show such a $\beta(B)$ relationship, like for the canonical weak itinerant superconductor $ScCo_2$ [66]. These results allow us to classify $Y_5Rh_{5.5}Pd_{0.5}Sn_{18}$ and $Y_5Rh_{5.5}Co_{0.5}Sn_{18}$ as CeSn₃- and/or $LuCo_2$ -type spin fluctuators, based on the classification proposed by Ikeda *et al.* in Ref. [66]. It is worth adding that the dc magnetic susceptibility χ shown in Fig. 15 as a plot of χ versus temperature and magnetic field is typical for this class of spin fluctuators.

Finally, we determine the Stoner enhancement factor $\alpha = 1 + 2/27\mu_s^2$ from the saturated value of μ_s (cf. Eq. (13) of Takeuchi and Masuda [48]). In the case of $Y_5Rh_{5.5}Pd_{0.5}Sn_{18}$, $\alpha = 1.00006$; e.g., for Sc_3In , Takeuchi and Masuda obtained $\alpha = 1.00015$. Once again, $Y_5Rh_{5.5}Pd_{0.5}Sn_{18}$ turns out to be a spin fluctuator with the closet value of α to the critical value $\alpha = 1$.

V. THEORETICAL APPROACH TO THE PEAK EFFECT IN $Y_{5-\delta}Rh_6Sn_{18}$ WITH LOCAL DISORDER AT Y OR Rh SITES

The observed PE can be explained by assuming that the vortex lattice starts to melt when approaching H_{c2} or T_c . Soft-

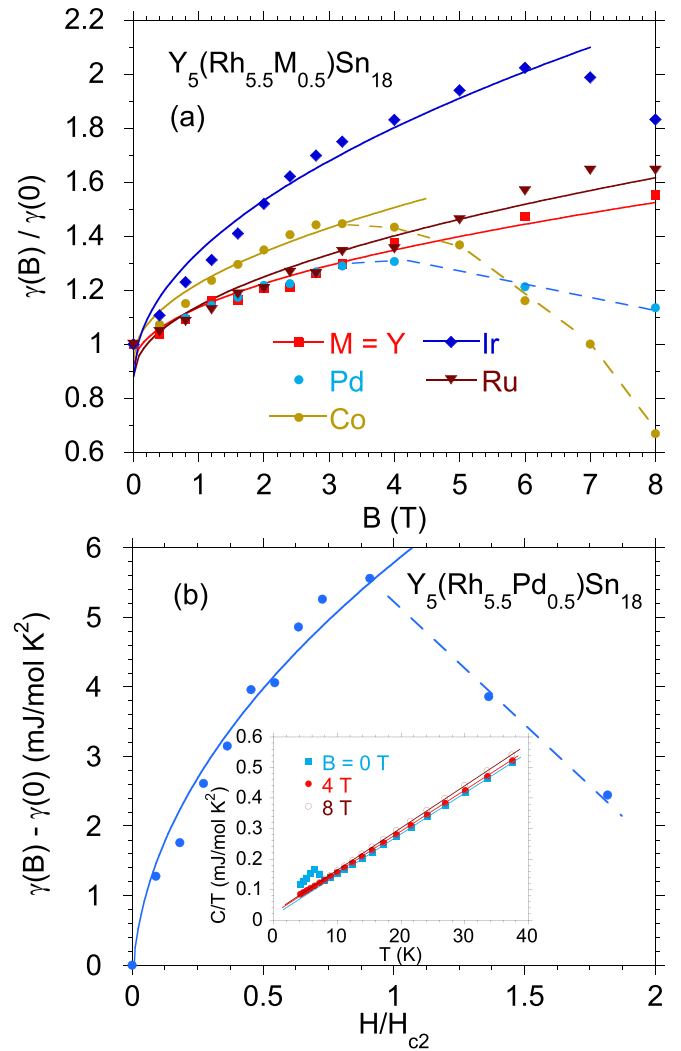


FIG. 14. (a) The electronic specific heat constant $\gamma_0^{(n)}$ in the normal state (n) vs magnetic field for $Y_5Rh_{5.5}M_{0.5}Sn_{18}$ ($M = Co, Ir, Ru, Pd$) in comparison to $\gamma_0^{(n)}$ of the reference $Y_5Rh_6Sn_{18}$ sample. The solid lines represent a fit to $\gamma(B) = \gamma(0) + \gamma' B^{1/2}$ expected for superconductors with a line node in the gap. The γ 's are normalized to the respective values of $\gamma_0^{(n)}$ for $B = 0$ (cf. Table II). (b) Sommerfeld parameter $\gamma(B)$ for $Y_5Rh_{5.5}Pd_{0.5}Sn_{18}$ as a function of magnetic field B . The data are well fitted by the expression $\gamma(B) = \gamma(0) + \gamma(H/H_{c2})^{0.5}$ for fields lower than H_{c2} . The inset displays the C/T vs T^2 at selected magnetic fields.

ening of the lattice allows single vortex lines to adjust their positions to be more effectively pinned by impurities and can lead to the PE. We recently proposed a simple toy model to explain the dependence of the vortex pinning strength on the radius of an impurity [18], which can explain the different magnitudes (or the absence) of the PE for different impurity atoms. By solving the Bogoliubov–de Gennes equations on a lattice deformed by impurity atom radius mismatch, we demonstrated an asymmetry in the pinning strength for impurity atoms larger than and smaller than the host atom. That is, the pinning as a function of the difference in radii for smaller impurities increases faster than for impurities larger than the host atom.

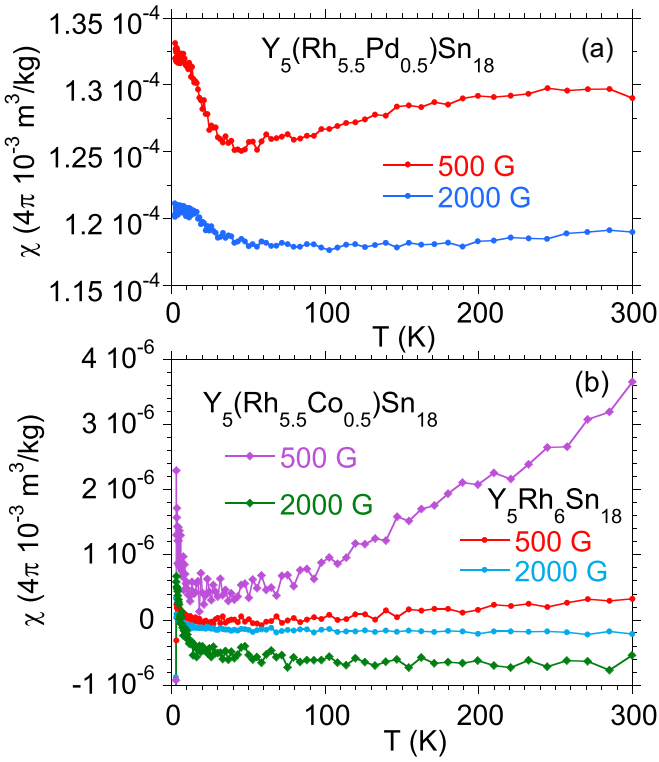


FIG. 15. The magnetic dc susceptibility at different magnetic fields for $Y_5Rh_{5.5}Pd_{0.5}Sn_{18}$ (a) and $Y_5Rh_{5.5}Co_{0.5}Sn_{18}$ (b), compared with the $\chi(T)$ for $Y_5Rh_6Sn_{18}$. The susceptibility for the Pd-doped sample is two orders of magnitude larger as compared with χ of the Co-doped sample.

To make the theoretical analysis semiquantitative here, we connect measured (macroscopic) characteristics of the samples with microscopic parameters which enter the model. In particular, we relate the local lattice deformation, described by the position-dependent hopping integral t_{ij} between the nearest-neighbor sites i and j , to the total volume change. Within the framework of the toy model, the hopping integral is given by

$$t_{ij} = t_0(1 + ae^{-br}), \quad (6)$$

where r is the distance between the center of the bond $i - j$ and the impurity site. The local deformation is parametrized with the parameter a , which defines the magnitude of the distortion, and b , which defines its size. We assume b to be such that t_{ij} differs significantly from t_0 only within a few lattice constants from the impurity site. To determine the magnitude a , we calculated how the average elementary cell volume changes with given substitutions. The results are presented in Table III.

Next, we construct a simple three-dimensional crystal model with harmonic interactions between the nearest- and the next-nearest-neighboring sites. Since we are interested only in the equilibrium configuration, this can be a good lowest-order approximation to more accurate potentials. For the parent compound, this is a cubic lattice of $L \times L \times L$ with all lattice constants a_0 . Then we randomly distribute substitutional impurities; that is, for a number of randomly chosen lattice sites, we replace a_0 with a_{imp} on all bonds between

TABLE III. Average relative change in elementary cell volume when substituting Rh atoms [$Y_5(Rh_{5.5}M_{0.5})Sn_{18}$] and Y atoms [$(Y_{4.5}M'_{0.5})Rh_6Sn_{18}$]. The change δv is defined as $\delta v = [V(YRhSn : M) - V(YRhSn)]/V(YRhSn)$. The corresponding cell volumes are given in Table I of this paper and in Table I of Ref. [18], respectively.

$Y_5(Rh_{5.5}M_{0.5})Sn_{18}$ M	$(Y_{4.5}M'_{0.5})Rh_6Sn_{18}$ M' [18]	δv
Co		-2.5×10^{-3}
Ru		-3.8×10^{-4}
Ir		$+9.6 \times 10^{-4}$
Pd		$+5.1 \times 10^{-3}$
	Ti	-1.4×10^{-2}
	Zr	-1.0×10^{-2}
	Lu	-1.7×10^{-3}
	Sr	$+6.3 \times 10^{-3}$

a given site and its neighbors. For the $Y_5(Rh_{5.5}M_{0.5})Sn_{18}$ and $(Y_{4.5}M'_{0.5})Rh_6Sn_{18}$ systems, the average concentration of substitutions is 1/58. The energy is given by

$$\mathcal{E} = \frac{K_1}{2} \sum_{\langle i,j \rangle} (|\vec{r}_i - \vec{r}_j| - a)^2 + \frac{K_2}{2} \sum_{\langle\langle i,j \rangle\rangle} (|\vec{r}_i - \vec{r}_j| - \sqrt{2}a)^2, \quad (7)$$

where \vec{r}_i is the position of the i th lattice site and

$$a = \begin{cases} a_{\text{imp}} & \text{if an impurity is located at site } i \text{ or } j \\ a_0 & \text{otherwise.} \end{cases}$$

Without the next-nearest-neighbor interaction, a rhomboid distortion would cost no energy.

In the next step, we allow the lattice to relax to its new energy minimum. In this process, the positions of the lattice sites are adjusted. Although the rearrangement of the lattice sites mostly concerns regions close to the impurities, the total volume of the lattice is also modified. When comparing the relative change of the total volume with the results presented in Table III, we can determine a_{imp} and the local deformation for all impurity atoms. This, in turn, allows one to use the toy model proposed in Ref. [18] to estimate the strength of the vortex pinning.

Since the energy of the lattice depends on its geometry (real positions of all the lattice sites), not on its topology, we cannot use periodic boundary conditions. Therefore, to minimize the finite-size effects, sufficiently large lattices need to be used in the simulations. Moreover, the simulations have to be averaged over a sufficient number of disorder realizations. Since for each disorder realization the lattice has to be relaxed, i.e., the interaction energy has to be minimized by fine-tuning the positions of all the lattice sites, the simulations are numerically very demanding. To make this task feasible, we used the stochastic gradient descent (SGD) method to minimize the lattice energy [67,68]. This method, which is used intensively in machine learning applications, provides a useful compromise between the computational complexity of individual algorithmic steps and the overall convergence rate [69].

In a practical realization, a $32 \times 32 \times 32$ lattice with 565 impurities was studied (Fig. 16). This number of impurities gives a density of impurities comparable to that of

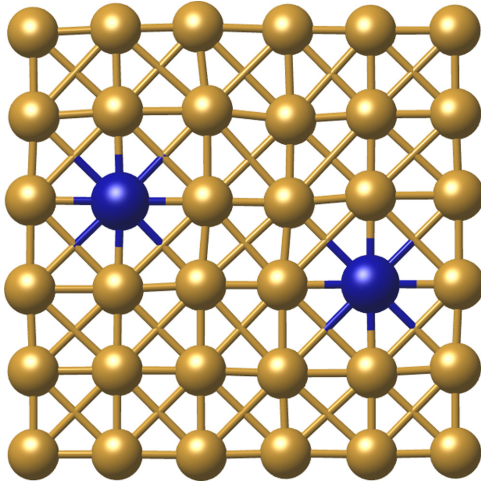


FIG. 16. An example of a $6 \times 6 \times 1$ part of a $32 \times 32 \times 32$ lattice with impurities. Two impurities with $a_{\text{imp}} = 1.1a_0$ [see Eq. (7)] located in this part are represented by the dark blue spheres. One can notice small deformations induced by the shown impurities as well as by impurities located in other parts of the lattice. The lines illustrate the nearest-neighbor and next-nearest-neighbor interactions taken into account in the model.

$\text{Y}_5(\text{Rh}_{5.5}\text{M}_{0.5})\text{Sn}_{18}$ and $(\text{Y}_{4.5}\text{M}'_{0.5})\text{Rh}_6\text{Sn}_{18}$. The length of the impurity bond a_{imp} was changed in a range tuned to generate the relative change of the total volume comparable to the values presented in Table III. For each value of a_{imp} , ten disorder realizations were randomly generated. For each realization, the SGD method was used to find the lattice configuration, which minimizes the interaction energy. Usually, 10^6 – 10^7 iterations were needed to achieve convergence of the relaxation process.

For $a_{\text{imp}} \neq a_0$ the sample is deformed, as illustrated in Fig. 17.

If $a_{\text{imp}} < a_0$ ($a_{\text{imp}} > a_0$), the volume is decreased (increased). We define the relative volume change as

$$\delta v = \frac{V(a_{\text{imp}}) - V(a_0)}{V(a_0)}, \quad (8)$$

where $V(a_0) = 32^3 a_0^3$ and $V(a_{\text{imp}})$ is the volume of a relaxed lattice with 565 impurities, averaged over random impurity distributions. The dependence obtained from δv on a_{imp} is represented by the blue line in Fig. 18(a). The relation is nonlinear, but for a small range of δv the nonlinearity is negligible. The red circles represent the volume change for different impurities (see Table III).

Figure 18(a) allows one to determine the parameter a_{imp} for different impurities. Then, assuming a simple relation for the hopping integral between the impurity and neighboring atoms,

$$t_{ij} = t_0 e^{c(a_0 - a_{\text{imp}})} \approx t_0 [1 + c(a_0 - a_{\text{imp}})], \quad (9)$$

and comparing with Eq. (6) one concludes that qualitatively

$$a \propto \frac{a_{\text{imp}}}{a_0} - 1, \quad (10)$$

where a is the parameter that enters the Bogoliubov–de Gennes equations that we use in the toy model [18] to estimate the pinning energy [see Eq. (6)]. The pinning energy is defined

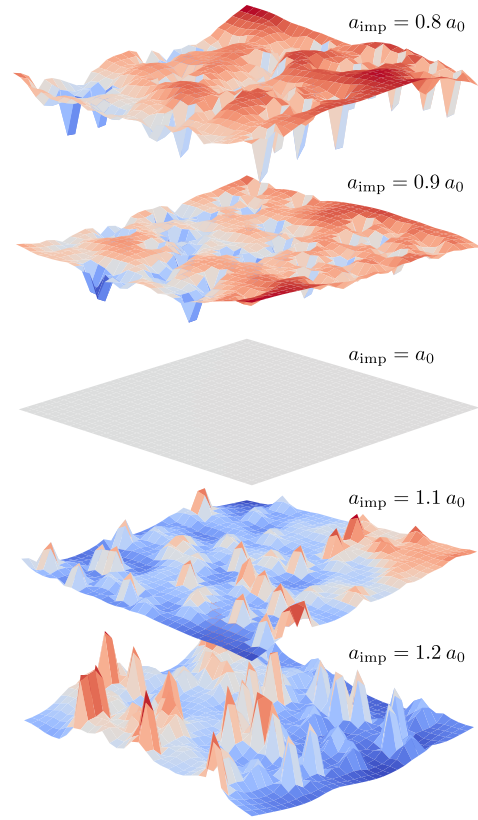


FIG. 17. Examples of the upper surface of a $32 \times 32 \times 32$ lattice with randomly distributed impurities for different a_{imp} . One may notice cavities for $a_{\text{imp}} < a_0$ and protrusions for $a_{\text{imp}} > a_0$. The magnitude of these features is strongly enlarged, but the scale is the same in all the plots (i.e., for all values of a_{imp}).

as the difference in the energy of a system with a vortex located at the position of an impurity and the energy of a system with a vortex at a large distance from the impurity. The more negative the difference, the stronger the pinning and the more pronounced PE can be expected. Since the relation between δv and a_{imp} is almost linear for the concentration of impurities used in the experiments, the pinning energy changes with the difference between the radius of the impurity and the radius of Rh or Y according to the way derived in Ref. [18]; i.e., the pinning energy increases with increasing radius difference, and for the same difference, the pinning is stronger if the impurity is smaller than the original atom. The predictions of this model agree with our experimental results, and therefore we can argue that the different magnitudes of the PE for different substitutions result from different strengths of vortex pinning, which, in turn, depend on the radius of the substitution.

VI. PE-LIKE BEHAVIOR IN THE AC MAGNETIC SUSCEPTIBILITY: COMMENTS

In the context of the PE phenomenon documented in the magnetoresistance of $\text{Y}_{5-\delta}\text{Rh}_{5.5}\text{M}_{0.5}\text{Sn}_{18}$ with dopants M significantly smaller (Co) or larger (Pd) than Rh (cf. Fig. 18), it is worth noting also a clear PE-like behavior in

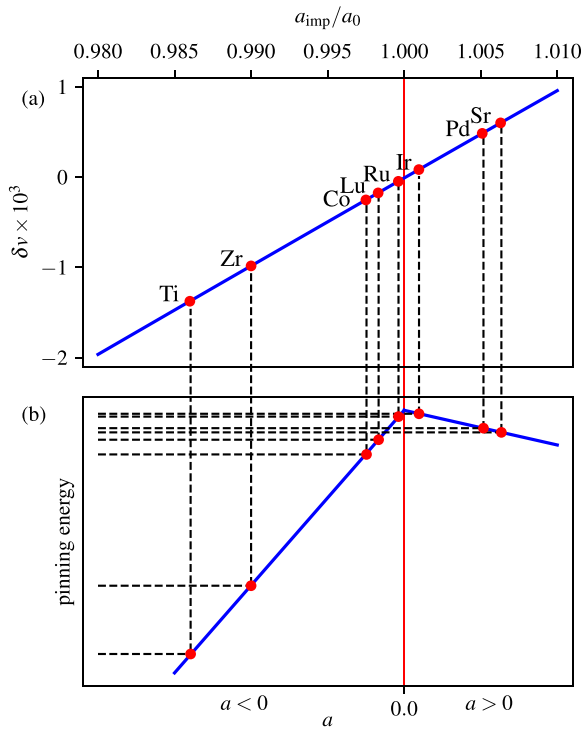


FIG. 18. (a) δv vs a_{imp} obtained from numerical simulations. The red circles represent volume changes for different impurities. (b) Schematic dependence of the pinning energy on parameter a [see Eq. (6)] adapted from Fig. 24 of Ref. [18]. Since only qualitative dependence is needed to order the pinning energies for different impurities, there are no numerical values marked on the axes. The dashed lines allow one to determine the pinning energy for given impurities (the pinning energy is negative; i.e., the strongest pinning is expected for Ti, and the weakest is expected for Ru and Ir). The vertical red line indicates parameters for a system without impurities.

the $\chi_{\text{ac}}(B)$ characteristics for the impurities $M = \text{Ir}$ and Ru , which are very close in size to the Rh atom, as well as for reference $\text{Y}_{5-\delta}\text{Rh}_6\text{Sn}_{18}$ with vacancies δ (see Fig. 11), while their accompanying magnetoresistance does not exhibit any significant abnormal properties at B^* , as shown in Fig. 8. Namely, $\chi_{\text{ac}}(B)$ exhibits here a much more pronounced PE-like anomaly at $B = B^*$ in contrast to the analogous magnetic anomaly, weakly observed in the χ_{ac} vs B isotherms for alloys with Co and Pd impurities in the Rh sites and/or Ti and Zr impurities in the Y sites. It seems that this PE-like anomaly, shown in Fig. 11 for $M = \text{Ir}$ or Ru and Rh , may occur for another reason. A similar type of anomaly in the $\sigma - B$ isotherms has been previously observed near H_{c2} , e.g., for the superconducting UPd_2Al_3 [70] and CeRu_2 [71] compounds, which at first glance appears to be similar to the celebrated PE. However, the authors excluded the nature of the vortex-pinning effect to explain this behavior. Within the possible mechanisms considered, the spin paramagnetic effect scenario seems to be a reasonable explanation. As the magnetic field is applied to a spin-singlet superconductor, the normal-state energy can be lowered by field-enhanced spin paramagnetism, and a transition towards the normal state may occur [72]. Alternatively, a modulated superconducting state, generally called the Fulde-Ferrell-Larkin-Ovchinnikov (FFLO) state,

may appear in applied fields close to H_{c2} [73–75]. However, the critical field $H_{c2} \sim 5.5$ T is almost three times larger than the field of the maxima in χ' either for $\text{Y}_{5-\delta}\text{Rh}_6\text{Sn}_{18}$ or its doped counterparts. This observation rather eliminates the FFLO scenario for $\text{Y}_{5-\delta}(\text{Rh}_{5.5}\text{M}_{0.5})\text{Sn}_{18}$.

VII. CONCLUDING REMARKS

The cubic skutteruditelike compounds of the formula $R_3M_4\text{Sn}_{13}$, where the metal R is extended by Ce or Yb , or their tetragonal equivalents $R_5M_6\text{Sn}_{18}$ ($R = \text{Sc}, \text{Y}, \text{Lu}$), have been known as a family of strongly correlated electron systems, attracting a great deal of attention over the past two decades due to their unique low-temperature characteristics [23,76–78] resulting from f - or d -electron correlations, as well as their promising thermoelectric properties [79] due to the existence of structural cages filled with Sn , R , and/or M atoms, respectively. However, the strong covalent bonding documented in these cages has ruled out the presence of rattling [80]; thus the measured value of figure of merit ZT is much lower than expected. However, the thermodynamic quantities and electrical conductivity of these materials reveal more and more anomalies in the range of both low and high temperatures.

In this paper, we focus on the $\text{Y}_{5-\delta}\text{Rh}_6\text{Sn}_{18}$ superconductor with vacancies δ at Y sites and atomic-scale disorder due to structural defects or by partial replacement of Y or Rh by metal M . This work complements the previously discussed issue of the presence of vortices generated by the field in the system of $(\text{Y}_{4.5-\delta}\text{M}'_{0.5})\text{Rh}_6\text{Sn}_{18}$ superconductors, when Y is substituted by Ti , Zr , La , Lu , and Sr . In this paper we have shown that a partial replacement of Rh by Co , Ru , Ir , or Pd also leads to a very similar magnetic-field-induced reentrance of superconductivity in $\text{Y}_{5-\delta}(\text{Rh}_{5.5}\text{M}_{0.5})\text{Sn}_{18}$ superconducting materials. In both cases, the nature of field-induced reentrance in superconductivity is the same; that is, the pinning strength depends on the atomic radii of the dopant and is observed to be the largest if the radius of M is much smaller than that of Y or Rh , respectively, while in the case of an inverse relationship between the radii of M and Y or Rh , the peak effect is observed to be much weaker. We assumed that the anomalous reentrance of superconductivity in the doped quasiskutterudites results from the stress located on the local defects (dopant and/or vacancy).

The experimental observations are modeled by a toy model in which the dependence of the pinning energy E_p on the size of the impurity M is computed. It was theoretically confirmed that the pinning energy increases with an increasing difference between the impurity radius and the radius of the host atom. However, the numerical simulations performed have shown that the lattice distortion produced by an impurity smaller than Y and/or Rh leads to a stronger pinning than that produced by a larger impurity. The resulting impact on flux lattice dynamics is responsible for the reentrant superconductivity and associated peak effect in samples with Zr , Ti , Sr , and Lu impurities at the Y sites and/or Co at Rh sites.

The second observation is the presence of spin fluctuation when $\text{Y}_{5-\delta}(\text{Rh}_{5.5}\text{M}_{0.5})\text{Sn}_{18}$ is doped with Co or Pd . The coexistence of SFs with superconductivity is rarely reported. In

this case, the low-temperature behavior is more complex and is accompanied by a peak effect as well.

Finally, we have found an M -dependent peak-effect-like anomaly in the χ_{ac} vs B data for the series of $Y_{5-\delta}(\text{Rh}_{5.5}\text{M}_{0.5})\text{Sn}_{18}$ samples; however, the magnitude of the *magnetic peak* exhibits the opposite behavior to that of a similar anomaly observed in the magnetoresistance of these samples. Namely, when the radii of M are very close to those of Rh, the *magnetic* PE-like behavior is strong, and the largest magnitude in the χ' anomaly is noted for $Y_{5-\delta}\text{Rh}_6\text{Sn}_{18}$ with vacancies $\delta \neq 0$, suggesting a different nature of this magnetic anomaly. Thus the χ_{ac} anomaly cannot be attributed to pinning. One of the possible explanations could be the presence of the spin paramagnetic effect [72] or, alternatively, the appearance of the FFLO state

[73–75]. The spin paramagnetic effect scenario seems to be more likely; however, at the current stage of research we are not able to clearly explain this anomaly.

ACKNOWLEDGMENTS

We are grateful to Krzysztof Rogacki for fruitful discussions. M.M.M. acknowledges support from the National Science Centre (Poland) under Grant No. DEC-2018/29/B/ST3/01892. Numerical calculations have been carried out using high-performance computing resources provided by the Wrocław Centre for Networking and Supercomputing. One of the authors (A.Ś.) thanks Agnieszka Ślebarska for valuable comments throughout the writing of this paper.

-
- [1] A. Ślebarski and M. M. Maška, *Materials* **13**, 5830 (2020).
- [2] A. Ślebarski, M. Fijałkowski, M. M. Maška, M. Mierzejewski, B. D. White, and M. B. Maple, *Phys. Rev. B* **89**, 125111 (2014).
- [3] A. Ślebarski, M. Fijałkowski, P. Zajdel, M. M. Maška, J. Deniszczyk, M. Zubko, O. Pavlosiuk, K. Sasmal, and M. B. Maple, *Phys. Rev. B* **102**, 054514 (2020).
- [4] T. Cren, D. Roditchev, W. Sacks, J. Klein, J.-B. Moussy, C. Deville-Cavellin, and M. Laguës, *Phys. Rev. Lett.* **84**, 147 (2000).
- [5] B. M. Andersen, A. Melikyan, T. S. Nunner, and P. J. Hirschfeld, *Phys. Rev. B* **74**, 060501(R) (2006).
- [6] M. B. Maple, P.-C. Ho, V. S. Zapf, N. A. Frederick, E. D. Bauer, W. M. Yuhasz, F. M. Woodward, and J. W. Lynn, *J. Phys. Soc. Jpn.* **71**(Suppl.), 23 (2002).
- [7] R. Vollmer, A. Faißt, C. Pfleiderer, H. v. Löhneysen, E. D. Bauer, P.-C. Ho, V. Zapf, and M. B. Maple, *Phys. Rev. Lett.* **90**, 057001 (2003).
- [8] G. Seyfarth, J. P. Brison, M.-A. Méasson, D. Braithwaite, G. Lapertot, and J. Flouquet, *Phys. Rev. Lett.* **97**, 236403 (2006).
- [9] M. E. McBriarty, P. Kumar, G. R. Stewart, and B. Andraka, *J. Phys.: Condens. Matter* **21**, 385701 (2009).
- [10] M.-A. Méasson, D. Braithwaite, G. Lapertot, J.-P. Brison, J. Flouquet, P. Bordet, H. Sugawara, and P. C. Canfield, *Phys. Rev. B* **77**, 134517 (2008).
- [11] A. Bianchi, R. Movshovich, M. Jaime, J. D. Thompson, P. G. Pagliuso, and J. L. Sarrao, *Phys. Rev. B* **64**, 220504(R) (2001).
- [12] J. S. Kim, D. J. Mixson, D. J. Burnette, T. Jones, P. Kumar, B. Andraka, G. R. Stewart, V. Craciun, W. Acree, H. Q. Yuan, D. Vandervelde, and M. B. Salamon, *Phys. Rev. B* **71**, 212505 (2005).
- [13] B. Liu, J. Wu, Y. Cui, H. Wang, Y. Liu, Z. Wang, Z. Ren, and G. Cao, *Supercond. Sci. Technol.* **31**, 125011 (2018).
- [14] P. W. Anderson, *J. Phys. Chem. Solids* **11**, 26 (1959).
- [15] A. A. Abrikosov and L. P. Gor'kov, *Zh. Eksp. Teor. Fiz.* **39**, 1781 (1961) [*Sov. Phys. JETP* **12**, 1243 (1961)].
- [16] M. N. Gastiasoro and B. M. Andersen, *Phys. Rev. B* **98**, 184510 (2018).
- [17] To distinguish M dopants at Y or Rh sites, we will use the label M' or M , respectively, or interchangeably we will use the following formulas: $(Y_{4.5}M'_{0.5})\text{Rh}_6\text{Sn}_{18}$ for M' dopants at Y sites and $Y_5(\text{Rh}_{5.5}\text{M}_{0.5})\text{Sn}_{18}$ for M impurities at Rh sites.
- [18] M. Fijałkowski, M. M. Maška, J. Deniszczyk, and A. Ślebarski, *Phys. Rev. B* **104**, 165306 (2021).
- [19] G. R. Stewart, Z. Fisk, J. O. Willis, and J. L. Smith, *Phys. Rev. Lett.* **52**, 679 (1984).
- [20] N. D. Mathur, F. M. Grosche, S. R. Julian, I. R. Walker, D. M. Freye, R. K. W. Haselwimmer, and G. G. Lonzarich, *Nature (London)* **394**, 39 (1998).
- [21] S. S. Saxena, P. Agarwal, K. Ahilan, F. M. Grosche, R. K. W. Haselwimmer, M. J. Steiner, E. Pugh, I. R. Walker, S. R. Julian, P. Monthoux, G. G. Lonzarich, A. Huxley, I. Sheikin, D. Braithwaite, and J. Flouquet, *Nature (London)* **406**, 587 (2000).
- [22] J. Yang, B. Chen, Ch. Michioka, and K. Yoshimura, *J. Phys. Soc. Jpn.* **79**, 113705 (2010).
- [23] L. E. Klintberg, S. K. Goh, P. L. Alireza, P. J. Saines, D. A. Tompsett, P. W. Logg, J. Yang, B. Chen, K. Yoshimura, and F. M. Grosche, *Phys. Rev. Lett.* **109**, 237008 (2012).
- [24] S. Miraglia, J. L. Hodeau, F. Bergevin, and M. Marezio, *Acta Crystallogr., Sect. B: Struct. Sci.* **43**, 76 (1987).
- [25] J. L. Hodeau, M. Marezio, and J. P. Remeika, *Acta Crystallogr., Sect. B: Struct. Sci.* **40**, 26 (1984).
- [26] J. Rodríguez-Carvajal, *Physica B (Amsterdam)* **192**, 55 (1993).
- [27] Y. Baer, G. Busch, and P. Cohn, *Rev. Sci. Instrum.* **46**, 466 (1975).
- [28] B. H. Toby, *Powder Diffr.* **21**, 67 (2006).
- [29] V. M. Goldschmidt, *Trans. Faraday Soc.* **25**, 253 (1929).
- [30] M. Gamza, W. Schnelle, A. Ślebarski, U. Burkhardt, R. Gumeniuk, and H. Rosner, *J. Phys.: Condens. Matter* **20**, 395208 (2008).
- [31] A. Ślebarski, M. Fijałkowski, M. M. Maška, J. Deniszczyk, P. Zajdel, B. Trump, and A. Yakovenko, *Phys. Rev. B* **103**, 155133 (2021).
- [32] A. Wang, Z. Y. Nie, F. Du, G. M. Pang, N. Kase, J. Akimitsu, Y. Chen, M. J. Gutmann, D. T. Adroja, R. S. Perry, C. Cao, M. Smidman, and H. Q. Yuan, *Phys. Rev. B* **103**, 024503 (2021).
- [33] J. Deniszczyk and A. Ślebarski, *Materials* **15**, 2451 (2022).
- [34] A. Ślebarski, P. Zajdel, M. M. Maška, J. Deniszczyk, and M. Fijałkowski, *J. Alloys Compd.* **819**, 152959 (2020).
- [35] Below the Fermi level, various bands are hybridized, giving for $Y_5\text{Rh}_6\text{Sn}_{18}$ the total DOS shown in Fig. 3. When $Y_5\text{Rh}_6\text{Sn}_{18}$ is

- doped with metal $M = \text{Co, Ru, Pd, or Ir}$, the Md -electron states are also hybridized with others, which in effect could slightly modify the TDOS. The XPS spectra obtained for pure Ru and Co metals exhibit a peak at the binding energy of about -2 eV (cf. Ref. [81]), which suggests an additional contribution of Ru or Co d -electron states to the total DOS of $\text{Y}_5\text{Rh}_6\text{Sn}_{18}$ when this parent compound is doped with metals M , respectively. As a result, the VB XPS spectra obtained for $\text{Y}_5\text{Rh}_{5.5}\text{Ru}_{0.5}\text{Sn}_{18}$ and $\text{Y}_5\text{Rh}_{5.5}\text{Co}_{0.5}\text{Sn}_{18}$ exhibit an increase in intensity at approximately -2 eV, when comparing them with the XPS bands of reference $\text{Y}_5\text{Rh}_6\text{Sn}_{18}$, as shown in Fig. 3. In contrast, the XPS spectra of pure Ir and Pd metals are more similar to those of pure Rh metal. Therefore the VB XPS spectra of $\text{Y}_5\text{Rh}_6\text{Sn}_{18}$ and $\text{Y}_5\text{Rh}_{5.5}\text{M}_{0.5}\text{Sn}_{18}$ ($M = \text{Pd and Ir}$) are almost identical, as shown in Fig. 3.
- [36] N. F. Mott, *Metal-Insulator Transitions* (Taylor and Francis, London, 1974).
- [37] N. F. Mott, *Philos. Mag.* **13**, 989 (1966).
- [38] A. Ślebarski, J. Goraus, and P. Witas, *Phys. Rev. B* **92**, 155136 (2015).
- [39] J. Spałek, A. Ślebarski, J. Goraus, L. Spałek, K. Tomala, A. Zarzycki, and A. Hackemer, *Phys. Rev. B* **72**, 155112 (2005).
- [40] K. Ueda and T. Moriya, *J. Phys. Soc. Jpn.* **39**, 605 (1975).
- [41] K. Ueda, *Solid State Commun.* **19**, 965 (1976).
- [42] A small η value gives a good fit to $C(T)/T$ data at $B = 3.2$ T with $\gamma_0 = 38$ mJ/mol K² and $\beta = 0.01$ J/mol K⁴; however, a good fit to $C(T)/T$ can also be obtained with $\eta = 0$ and $\gamma_0 = 30$ mJ/mol K² and $\beta = 0.014$ J/mol K⁴ contributions. In both cases, the $C(T)/T$ vs T^2 change is linear and looks the same. We, however, decided to present the C/T low- T data approximated with the SF expression because of the following reasons, even though the SF effect is very weakly visible in the specific heat data. $C(T)/T$ is not expressed by the SF contribution to the specific heat for Ir, Ru, and Rh dopants ($\eta = 0$). We also would like to emphasize that the effect of SF, clearly visible in the temperature dependence of $\chi(T)$ and $\rho(T)$ data, can also be applied in the low- $TC(T)$ data. We noted that the SF contribution enhances γ_0 , which is expected.
- [43] B. Zeimet, B. Glowacki, and J. Evetts, *Eur. Phys. J. B* **29**, 359 (2002).
- [44] D. Bucheli, S. Caprara, C. Castellani, and M. Grilli, *New J. Phys.* **15**, 023014 (2013).
- [45] D. Saint-James and P. D. de Gennes, *Phys. Lett.* **7**, 306 (1963).
- [46] M. Strongin, A. Paskin, D. G. Schweitzer, O. F. Kammerer, and P. P. Craig, *Phys. Rev. Lett.* **12**, 442 (1964).
- [47] S. Ogawa, *J. Phys. Soc. Jpn.* **40**, 1007 (1976).
- [48] J. Takeuchi and Y. Masuda, *J. Phys. Soc. Jpn.* **46**, 468 (1979).
- [49] Y. Yamaguchi, Y. Nishihara, and S. Ogawa, *J. Magn. Magn. Mater.* **31-34**, 513 (1983).
- [50] T. P. Orlando, E. J. McNiff, Jr., S. Foner, and M. R. Beasley, *Phys. Rev. B* **19**, 4545 (1979).
- [51] E. Helfand and N. R. Werthamer, *Phys. Rev. Lett.* **13**, 686 (1964); N. R. Werthamer, E. Helfand, and P. C. Hohenberg, *Phys. Rev.* **147**, 295 (1966).
- [52] P. E. Seiden, *Phys. Rev.* **179**, 458 (1969).
- [53] P. Morel and P. W. Anderson, *Phys. Rev.* **125**, 1263 (1962).
- [54] W. L. McMillan, *Phys. Rev.* **167**, 331 (1968).
- [55] J. J. Hopfield, *Phys. Rev.* **186**, 443 (1969).
- [56] W. F. Brinkman and S. Engelsberg, *Phys. Rev.* **169**, 417 (1968).
- [57] M. T. Beal-Monod, S.-K. Ma, and D. R. Fredkin, *Phys. Rev. Lett.* **20**, 929 (1968).
- [58] P. Hertel, J. Appel, and D. Fay, *Phys. Rev. B* **22**, 534 (1980).
- [59] R. J. Trainor, M. B. Brodsky, and H. V. Culbert, *Phys. Rev. Lett.* **34**, 1019 (1975).
- [60] K. Ikeda and K. A. Gschneidner, Jr., *Phys. Rev. Lett.* **45**, 1341 (1980).
- [61] N. Kase, K. Inoue, H. Hayamizu, and J. Akimitsu, *J. Phys. Soc. Jpn.* **80**, SA112 (2011).
- [62] A. Bhattacharyya, D. Adroja, N. Kase, A. Hillier, J. Akimitsu, and A. Strydom, *Sci. Rep.* **5**, 12926 (2015).
- [63] Z. Zhang, Y. Xu, C. N. Kuo, X. C. Hong, M. X. Wang, P. L. Cai, J. K. Dong, C. S. Lue, and S. Y. Li, *Supercond. Sci. Technol.* **28**, 105008 (2015).
- [64] G. E. Volovik, *Pis'ma Zh. Eksp. Teor. Fiz.* **58**, 457 (1993) [*JETP Lett.* **58**, 469 (1993)].
- [65] M. Feig, W. Schnelle, A. Maisuradze, A. Amon, Ch. Baines, M. Nicklas, S. Seiro, L. Howald, R. Khasanov, A. Leithe-Jasper, and R. Gumeniuk, *Phys. Rev. B* **102**, 024508 (2020).
- [66] K. Ikeda, S. K. Dhar, M. Yoshizawa, and K. A. Gschneidner, Jr., *J. Magn. Magn. Mater.* **100**, 292 (1991).
- [67] H. Robbins and S. Monroe, *Ann. Math. Stat.* **22**, 400 (1951).
- [68] L. Bottou and Y. LeCun, *Adv. Neural Inf. Process. Syst.* **16**, 217 (2004).
- [69] Y. Amit and U. Grenander, *J. Multivariate Anal.* **37**, 197 (1991).
- [70] F. Steglich, C. Geibel, K. Gloos, P. Hellmann, R. Kohler, M. Lang, R. Modler, and C. Schank, *Physica C (Amsterdam)* **235-240**, 95 (1994).
- [71] S. B. Roy, A. K. Pradhan, and P. Chaddah, *Phys. Rev. B* **52**, R9847 (1995).
- [72] T. Terashima, N. Kikugawa, A. Kiswandhi, E.-S. Choi, K. Kihou, S. Ishida, C.-H. Lee, A. Iyo, H. Eisaki, and S. Uji, *Phys. Rev. B* **99**, 094508 (2019).
- [73] K. Maki, *Phys. Phys. Fiz.* **1**, 127 (1964); **1**, 201(E) (1964).
- [74] P. Fulde and R. A. Ferrell, *Phys. Rev.* **135**, A550 (1964).
- [75] A. I. Larkin and Y. Ovchinnikov, *Zh. Eksp. Teor. Fiz.* **47**, 1136 (1964) [*Sov. Phys. JETP* **20**, 762 (1965)].
- [76] E. L. Thomas, H.-O. Lee, A. N. Bankston, S. MaQuilon, P. Klavins, M. Moldovan, D. P. Young, Z. Fisk, and J. Y. Chan, *J. Solid State Chem.* **179**, 1642 (2006).
- [77] C. S. Lue, H. F. Liu, S.-L. Hsu, M. W. Chu, H. Y. Liao, and Y. K. Kuo, *Phys. Rev. B* **85**, 205120 (2012).
- [78] A. Ślebarski, J. Goraus, P. Witas, L. Kalinowski, and M. Fijałkowski, *Phys. Rev. B* **91**, 035101 (2015).
- [79] U. Köhler, A. P. Pikul, N. Oeschler, T. Westerkamp, A. M. Strydom, and F. Steglich, *J. Phys.: Condens. Matter* **19**, 386207 (2007).
- [80] L. Kalinowski, M. Kądziołka-Gaweł, and A. Ślebarski, *Phys. Rev. B* **98**, 245140 (2018).
- [81] <https://xpslibrary.com/valence-band-spectra-elements>.